Studies on Astrophysical Nuclides Far From Stability

Studies on Astrophysical Nuclides Far From Stability with Numerical Simulations and Systematics

By

Johnson Liang, B.Sc.

A Thesis

Submitted to the School of Graduate Studies

in Partial Fulfilment of the Requirements

for the Degree

Master of Science

McMaster University

©Copyright by Johnson Liang, September 2016

Master of Science (2016) McMaster University

(Physics and Astronomy) Hamilton, Ontario

TITLE: Studies on Astrophysical Nuclides Far From Stability with Numerical Simulations and Systematics

AUTHOR: Johnson Liang, B.Sc. (McMaster University)

SUPERVISORS: Alan Chen

NUMBER OF PAGES: ix, 91

Abstract

Explosive events in our universe provide an environment where rare nucleosynthesis events can occur. Understanding the mechanisms and processes during these events is integral to understanding the relative abundances of the elements in our universe. The rapid neutron capture process or r-process is thought to be responsible for producing approximately half of the heavy elements in our universe. A critical input in the calculation of r-process nucleosynthesis is the β^- - delayed neutron (βDN) emission probability, P_n. However theoretical calcuations of P_n have not been successful in reproducing experimental values. A semi-empirical formula using systematics can be adopted, which can give an approximate P_n value for unmeasured precursors. To complete this, we carried out a comprehensive evaluation of P_n and half life,$T_{1/2}$ values from literature, which we present in this work in a table of recommended values for the range Z=30-40,49,50. Two methods of identifying systematics in neutron emission probability P_n (McCutchan et al. 2012),(Kratz,Herrmann, 1988) are compared using the evaluated values, wherein the McCutchan et al. method was significantly more accurate than the Kratz-Herrmann method, and especially so in the lower Q regions. In this work we also explore classical novae and present a sensitivity study on classical nova nucleosynthesis endpoint nuclei. The reaction rates of ^{36}Ar,^{37}Ar and ^{40}K were of particular interest as they showed the largest impact on the final abundances.

Acknowledgements

Thanks to Alan Chen, for all of your insight both in and out of science. To Balraj Singh, for all your knowledge and encouragement.

To my parents, Tho and My Chau, for teaching me the value of hard work. To my brother, Carson, for all of his support through the years.

To Michael Birch, for your dedication and our discussions. And finally, to all the friends: The most profound memories will be of the sleepless nights completing assignments, raising glasses at the phoenix and all of our wonder at the curiosities in the universe.

Table of Contents

List of Figures

List of Tables

Chapter 1

Introduction: β - Delayed Neutron Emission

1.1 R-Process

Along with the s-process, the r(apid)-process is a mechanism by which nuclides past the iron peak can be synthesized. The main difference is that it is assumed the environmental neutron density and temperature are much higher in the r-process compared to the s-process ($N_n \geq 10^{20}$ cm^{-3}, $T \geq 1$ GK) (2011 Arcones and Martinez-Pinedo). As a result, a nuclide can undergo additional neutron captures before β^- decay or neutron emission occurs. This drives matter towards the neutron rich side of the table of nuclides and are proton deficient when compared to s-process products (Iliadis, 2015). In this environment, neutron capture and photodisintegration reactions [(n, γ) and (γ, n)] are much faster than the β^- decays of the heavy nuclei (Iliadis, 2015).

The simplest equation for the time evolved evolution of the abundance of a seed nucleus,$^{\mathrm{A}}{}_{\mathrm{Z}}X$, such as ^{56}Fe is as follows:

$$\frac{dN(Z,A)}{dt} = -N_n N(Z,A) < \sigma v >_{Z,A} + N(Z,A+1)\lambda_\gamma(Z,A+1) \tag{1.1}$$

where N_n is the neutron density, N(Z,A) represents the abundance of the seed nuclei, $< \sigma v >$ is the reaction rate per particle pair for neutron capture, and λ_γ(Z,A+1) is the decay constant for isotope $^{\mathrm{A+1}}{}_{\mathrm{Z}}X$. One can assume for sufficiently large N_n and T, that after a long time, the abundance outflow from neutron capture and inflow from photodisintegration will be approximately equal, and a steady flow will be achieved (1982 Cameron, Cowan and Truran), that is:

$$N_n N(Z,A) < \sigma v >_{Z,A} \approx N(Z,A+1)\lambda_\gamma(Z,A+1) \tag{1.2}$$
$$\frac{dN(Z,A)}{dt} \approx 0$$

The abundance ratios can then be expressed as a statistical equation, namely the Saha equation (1920 Saha):

$$\frac{N(Z,A+1)}{N(Z,A)} = N_n \Big(\frac{h^2}{2\pi m_{An} kT}\Big)^{3/2} \frac{(2j_{Z,A+1}+1)}{(2j_{Z,A}+1)(2j_n+1)} \frac{G^{\mathrm{norm}}{}_{\mathrm{Z,A+1}}}{G^{\mathrm{norm}}{}_{\mathrm{Z,A}}} e^{Q_{n\gamma}/kT} \tag{1.3}$$

where G^{norm} is the normalized partition function, (which has been normalized to unity), j is the spin of the particle, which in turn gives us the statistical weight of the particle. $Q_{n\gamma}$ is the Q value of the forward reaction which is synonymous with the neutron separation energy of the daughter nuclei, since the energy released by this reaction is the same amount needed to complete the re-

verse photodisintegration reaction (Iliadis, 2015). m_{An} represents the reduced mass.

From this equation the number abundance of a single isotope relative to an adjacent isotope can be established, and through successive applications of the Saha equation, one can find the abundance of any isotope within a single isotopic chain (Iliadis, Iliadis).

Generally, the $Q_{n\gamma}$ value is relatively high when near the valley of stability. According to Eqn. 1.3 this implies N(Z,A+1) $>$ N(Z,A), or in other words, the neutron capture rate is stronger than the photodisintegration rate near the valley of stability. Conversely, near the neutron dripline, $Q_{n\gamma}$ will be relatively small. This implies that N(Z,A+1) $<$ N(Z,A), or that photodisintegration will prevent neutron capture from progressing further. Consequently, this implies that there will be a certain $Q_{n\gamma}$ value where the photodisintegration rate matches the neutron capture rate and at that value, there will be an abundance maximum, and the abundance will build up at that isotope. The position of this maximum can be affected by the temperature and neutron density, in accordance with Eqn. 1.3.

Another factor that affects $Q_{n\gamma}$ is the even/odd neutron pairing interaction. Nuclides with an even number of neutrons will have smaller Q values than those that have an odd number of neutrons. Nucleons within the nucleus tend to pair together in a configuration of opposing spins. In nuclei with even numbers of neutrons, the nucleons are all paired together which results in a total momentum of J=0 for their ground states. For odd numbers of neutrons, a final nucleon can go unpaired, leading to a non-zero momentum in the nu-

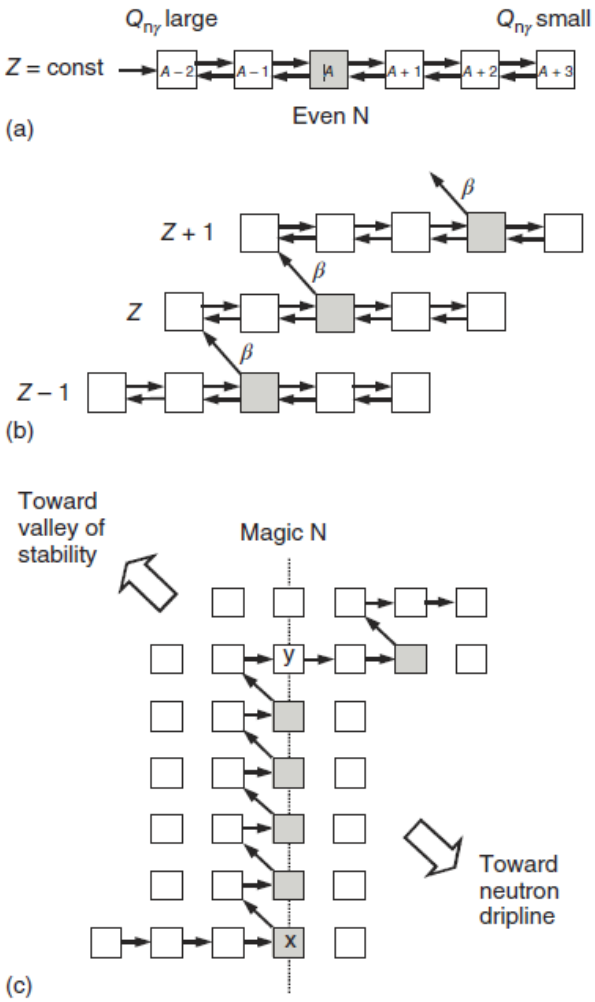

Figure 1.1 a) shows an isotopic chain in (n,γ),(γ,n) equilibrium (waiting point approximation), with abundance maximum at the shaded square. b) shows the β^- decays of waiting point nuclei. c) shows a special case of the waiting point approximation at a neutron magic number. Figure from (Iliadis, 2015).

cleus and higher.This will result in even-N isotopes becoming the maxima in the abundance evolution. Thus, even-N nuclides with the specific $Q_{n\gamma}$ that balances photodisintegration and neutron capture then represent "waiting points" where the only way to progress is through a β^--decay which will branch the nucleosynthesis flow to other isotopic chains. A schematic of these features of the flow is given in Fig. 1.1 (a),(b). The total probability of β^- decay from one isotopic chain is given by:

$$\gamma_z \equiv \sum_A (N(Z,A)/N_Z)\gamma_\beta(Z,A) \tag{1.4}$$

where the abundance distribution in the chain has been normalized to the total abundance, N_Z, and γ_β is the β decay constant.

A general equation to describe the time evolution of an element (Z,A) in the waiting point approximation is given by:

$$\frac{dN_Z}{dt} = -\gamma_Z N_Z + \gamma_{Z-1} N_{Z-1} \tag{1.5}$$

The first term describes the decay of the element (Z,A) through β^- decay, while the second term is the production through the β^- decay of element (Z-1,A). This relationallows the calculation of abundances of entire isotopic chains, while the Saha equation yields isotopic abundances within an isotopic chain.

Another factor that must be included is the possibility of a nucleus with a full neutron shell, or nuclei posessing a magic number of neutrons. Consider an isotope X, which has a full neutron shell. The Q value of (n,γ)X reaction will be relatively large compared to Q value of the X(n,γ) reaction. When

the abundance flow reaches this member of the isotopic chain, it will not be able to progress further through neutron capture. Thus, the nucleus at this point will be forced to undergo β^- decay to move through the r-process path. Interestingly, following a β^- decay of a nucleus with magic neutron number, the subsequent neutron capture will move it back to that neutron magic number and the abundance flow will move along the isotones, travelling up vertically in Z number towards the valley of stability as illustrated in Fig. 1.1 (c) and Fig. 1.2. On the r-process path, half-lives are typically on the order of $T_{1/2} \approx 0.01 - 0.05s$ (Iliadis, 2015), but at these magic neutron number nuclei, this time can be significantly longer, causing a build-up in abundance until it is able to β^- decay (Iliadis, 2015).These points are noticeable waiting point nuclei and have a profound effect on the final abundances.

Once the nucleus reaches the point y on Fig. 1.1c) the half life becomes long enough that neutron capture can occur again.

Of these waiting point nuclei, the most important are ^{80}Zn, ^{130}Cd and ^{195}Tm (Kratz et al. 1988). This is because moving to stability will increase the Q value, eventually allowing the r-process to resume neutron-capture. These nuclei represent the final waiting point nuclei before neutron-capture resumes. Additionally, because they are the closest to stability, they have the longest half-lives of the waiting point nuclei, meaning the abundances near these locations will accumulate before neutron flux terminates (Iliadis, 2015).After cessation of the neutron flux, the resultant products can begin to β^- decay or undergo a neutron emission towards stability. It is thought that the three main residual abundance peaks at A $\approx$ 80,130, and 195 in Fig. 1.3 are asso-

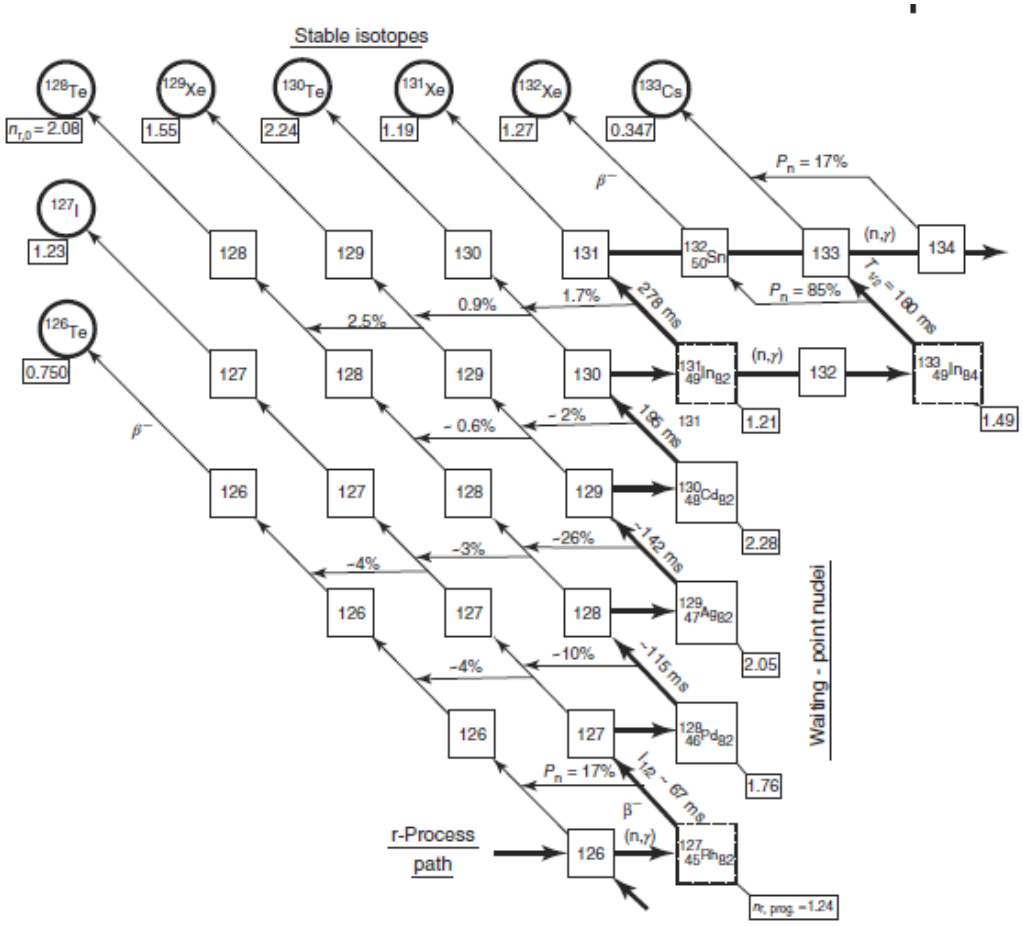

Figure 1.2 Decay pathways for neutron number N=82. β^- decay half lives are shown along the diagonal arrows. The β^- delayed neutron decay probabilities are shown along the horizontal lines. Figure from (Iliadis 2015), cited from (Kratz et al.,1988).

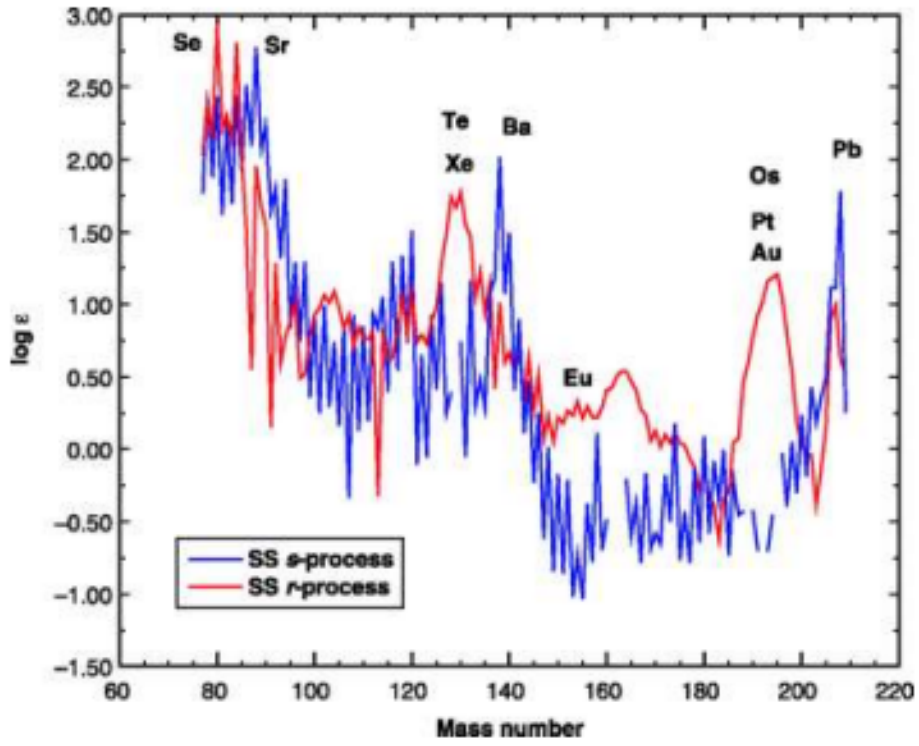

Figure 1.3 breakdown of r- and s-process abundances from solar system (meteoric) values. Figure from (Sneden, Cowan, 2003).

ciated with the N=50,82 and 126 closed shells (Mumpower 2015) during the r-process.

The site of the r-process is still a hotly debated subject. There are two astrophysical environments that are strong candidates for this process. The first site is core collapse supernovae and the resulting neutrino-driven wind. At the end of a massive star's lifetime, the core becomes so dense that electron degeneracy is unable to balance the inwards gravitational force. Following a core-collapse, a massive amount of gravitational energy is released via 2 shock-

waves: an initial "bounce" from the collapse of material and a delayed electron neutrino and antineutrino shockwave from the proto-neutron star (Arcones, A. and Martínez-Pinedo, G., 2011)(Duncan, R. C. and Shapiro, S. L. and Wasserman, I., 1986). The delayed shockwave is important to nucleosynthesis as the flux of neutrinos and antineutrinos drive a continuous flow of neutrons and protons out towards the earlier supernova ejecta. If that flux is neutron rich, it could give rise to the production of neutron rich nuclei but simulations of this event fail to produce the necessary abundances of heavy nuclei, in particular the third r-process abundance peak at A=195. The second site is a merger of either two neutron stars or a neutron star and a black hole. A problem with this scenario is that the event rate is too low and the required mass ejected per event would be too large to be consistent with observations (Iliadis, 2015).

Another aspect of the study of the r-process is the modeling of the atomic nuclei. An important step was the improvement of the theoretical description of nuclear masses (1995 Möller et al.), and microscopic approaces to the β-decay strength function. The improvements to the latter include the i) the Quasi-particle Random Phase Approximation (QRPA) with no T=0 proton-neutron pairing, employing the ground-state description from the finite-range droplet model (FRDM) (Möller, Pfeiffer, and Kratz 2003) ii) continuum proton-neutron QRPA based on the self-consistent density functional theory (DF3+cQRPA) (I.N. Borzov 2003), iii) the interacting shell model (Zhi et al. 2013) and iv) the fully self-consistent covariant density functional theory (Marketin et al. 2016), however, a detailed description is beyond the scope of this project. Another major step was the realization that first-forbidden (FF) transitions results in a shortening of β-decay half-lives of neutron rich nuclei near

full neutron shells mainly around N=50,82 and 126. In general, nuclear masses, which are used to calculate $Q_{n\gamma}$ determine the path of the r-process through the table of nuclides, while the β decay rates determine speed of progression. Finally, the combination of β decay, neutron capture and β-delayed neutron emission play a crucial role in shaping the final abundance distribution.

1.2 β-Delayed Neutron Emission

An important factor that affects the final abundances in the r-process as shown in Fig. 1.2 is β^--delayed neutron emission. Following a β^- decay, the energy release depends on the change in atomic masses before and after the interaction.

$$Q_{\beta^-} = (m({}^{\mathrm{A}}_{\mathrm{Z}}X_N) - m({}^{\mathrm{A}}_{\mathrm{Z+1}}X_{N-1}))c^2 \tag{1.6}$$

This energy is distributed in several ways, such as the kinetic energy of the electron, total energy of the neutrino and transitions to excited states in the nuclei. Sometimes, a beta decay can populate a level that exceeds the neutron separation energy, S_n, that is $Q_{\beta n} = Q_\beta - S_n > 0$. This causes the daughter nucleus to be unstable, which leads to a neutron emission, or β^--delayed neutron emission. These emissions compete with transitions to the bound states which will gamma decay down to the ground states of the β-decay daughter nucleus. A schematic of this is shown in Fig. 1.4

It is also possible to undergo additional neutron emissions if the daughter nucleus is excited to an energy level higher than its neutron separation energy,

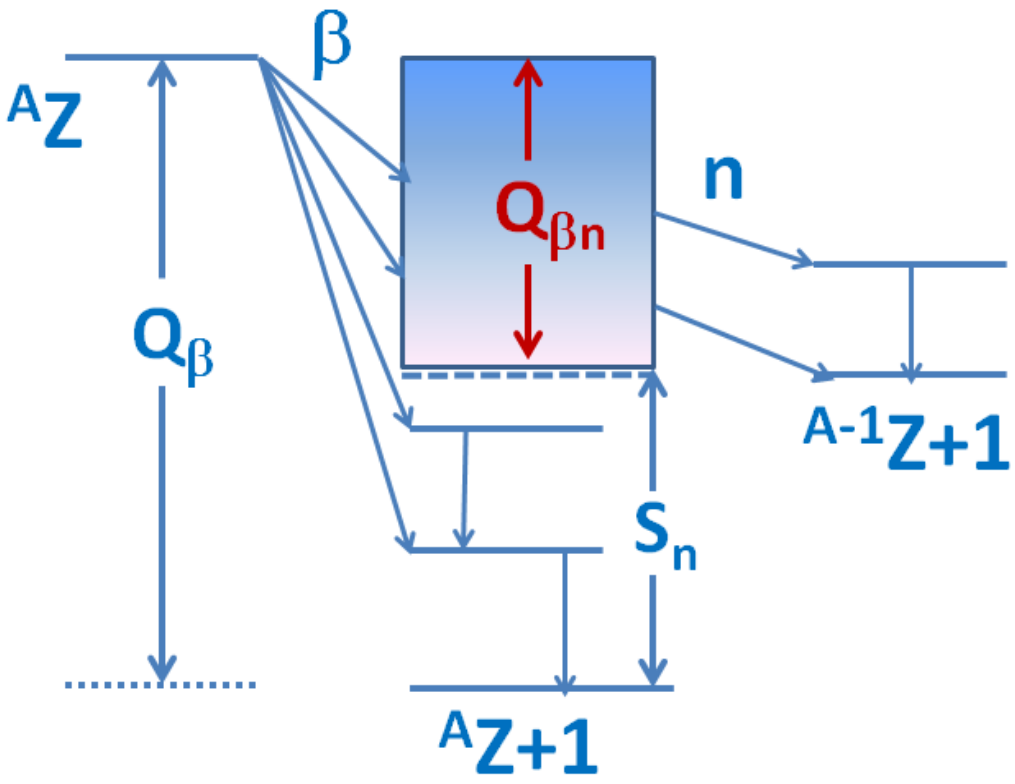

Figure 1.4 Schematic for β^--delayed neutron emission. If the Q_β of the reaction is greater than the neutron separation energy, S_n, then it is possible for a transition to a neutron unbound state, leading to neutron emission.

and further, if the grand-daughter nucleus is also excited to an energy higher than its neutron separation energy, a subsequent neutron emission can occur, and so on. In general, the energy required to separate x neutrons is given by S_{xn}, which is the sum of the neutron separation energies for the x neutron separations.

An important property to quantify is the probability of neutron emission, or P_n, which occurs in Fig. 1.2 along horizontal lines. These paths allow for branching to different isotopic chains and ultimately affect the distribution of final abundances. Multiple neutron emission probability - that is the probability of $x-1$ subsequent emissions after the first - can be defined as P_{xn} where x is the number of neutrons being emitted. These probabilities are related to the β-decay strength distribution, but there is a large discrepancy in microscopic/macroscopic models compared to experimental data (Möller et al. 1995). Phenomenological models can also be used to determine P_n values which will be discussed in the next section, but are subject to uncertainties of about a factor of 2 (Caballero-Folch et al. 2016). These can predict the P_n values up to an order of magnitude, which are not good enough to make accurate predictions. Overall, the understanding of β-delayed neutron emission is quite poor, and there is a need to improve models in order to extrapolate data to precursors with unknown P_n values.

Experimental P_n values have been determined for just over 200 nuclei, out of the more than 600 which are energetically possible (McCutchan et al. 2014). There is currently an effort to produce more experimental measurements of these values. Radioactive beam facilities that can produce intense, high quality,

accelerated beams of short lived isotopes, are required to measure P_n values. These can be found at institutions such as Catania (Italy), GANIL (France), RIKEN (Japan), CERN (Switzerland), GSI (Germany), MSU (USA), ORNL (USA), Texas A+M (USA), and TRIUMF (Canada) (B.R Fulton 2011). In addition, many of these accelerators are being built that are dedicated to the study of radioactive isotope beams, and are planned to come into operation within the next decade (B.R Fulton 2011).

1.3 Systematics of β-Delayed Neutron Emission

Theoretical calculations of unmeasured β^--delayed neutron emission probabilities have been attempted, but because they are sometimes dependent on nuclear properties that must be extrapolated, they may not be reliable (Kratz, 1988). An alternative is to determine the probabilities from a semi-empirical formula extracted from the systematic evaluation of P_n for known nuclides. To begin, a simple correlation between the P_n and the energy window, $(Q_\beta - S_n)$, was established by Amiel and Feldstein (Amiel and Feldstein, 1969):

$$P_n \approx a(Q_\beta - S_n)^b \tag{1.7}$$

where n and a are constants determined from fits to the available experimental data. Fig. 1.5 shows this correlation between P_n and $(Q_\beta - S_n)$ on a log-log scale. A line of best fit with slope, $n = 1.65(24)$ with lines of standard deviation, σ and 2σ are shown.

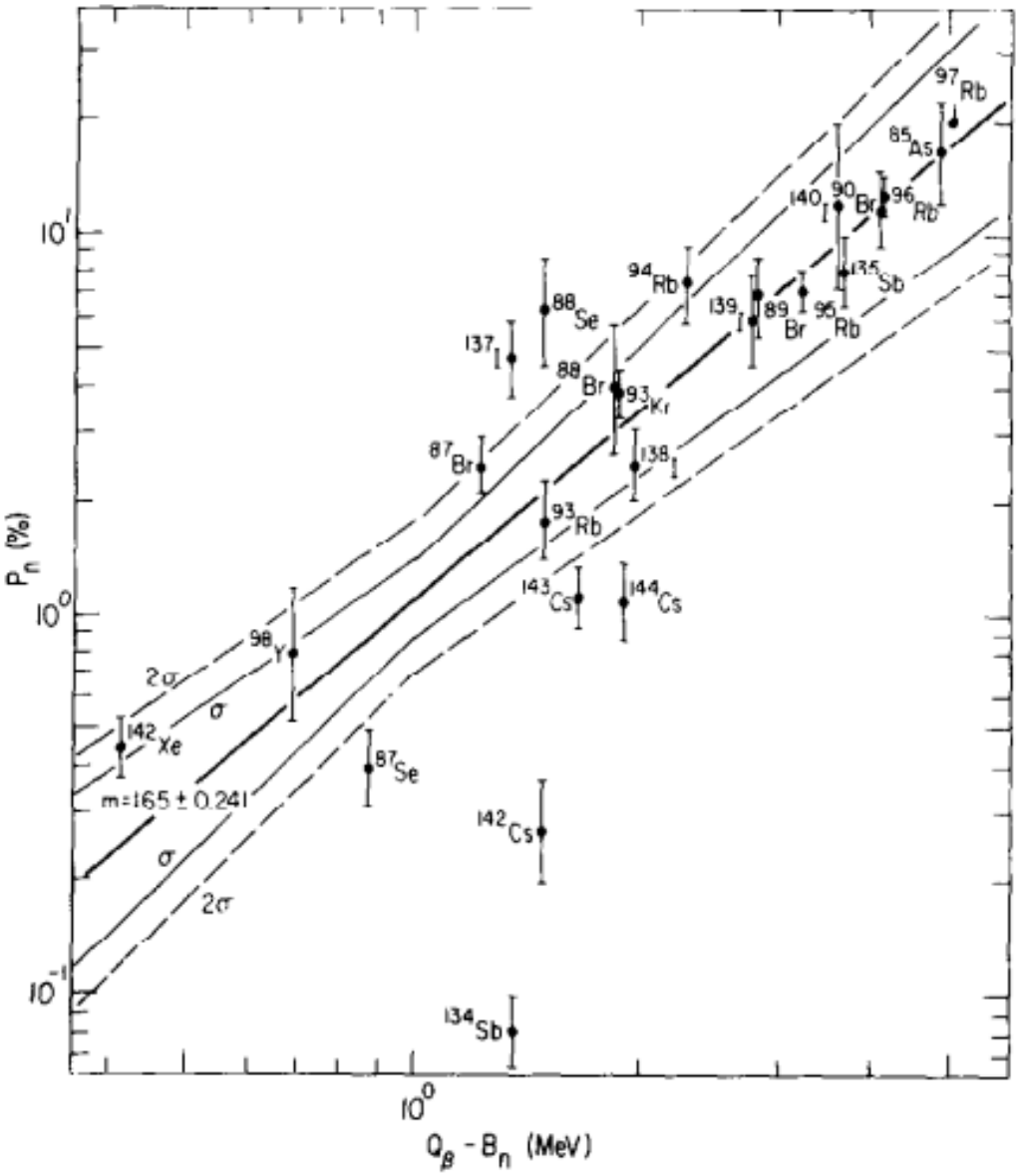

Figure 1.5 Correlation of experimental neutron emission probabilities with energy window using data published until July 1969 for isotopes with values of $(Q_\beta - S_n) > 0.4MeV$ and $P_n > 0.07$. A line of best fit with slope, $n = 1.65(24)$ with lines of standard deviation, σ and 2σ are shown. Figure from (Amiel and Feldstein, 1969).

A more constrained treatment of this formula was given by Kratz and Herrmann (Kratz and Herrmann, 1973). It begins with the equation for P_n in terms of beta-decay quantities:

$$P_n = \frac{\int_{S_n}^{Q_\beta} f(Z, Q_\beta - E) S_\beta(E) \Gamma_n / \Gamma_{tot} dE}{\int_0^{Q_n} f(Z, Q_\beta - E) S_\beta(E) dE} \tag{1.8}$$

where $f(Z, Q_\beta - S_n)$ is the Fermi function, Γ_n is the neutron width, Γ_{tot} is the sum of the neutron and gamma widths, and S_β is the β strength function.

Assumptions can be made to simplify this equation. The first is that the gamma decay competing with neutron decay can be neglected (Kratz and Herrmann, 1973), that is:

$$\Gamma_n / \Gamma_{tot} \approx 1 \tag{1.9}$$

The β strength function can be approximated as a constant for values of E that are below a cut-off energy based on even-odd pairing interactions, and zero otherwise (Hørnshoj et al. 1972).
Eqn. 1.8 then becomes:

$$P_n = \frac{\int_{S_n}^{Q_\beta} f(Z, Q_\beta - E) S_\beta(E) dE}{\int_0^{Q_\beta} f(Z, Q_\beta - S_n) S_\beta(E) dE} \tag{1.10}$$

Finally, the Fermi function can be approximated as $(Q_\beta - S_n)^b$ (Kratz and Herrmann, 1973), and solving this leads to the Kratz-Herrmann equation:

$$P_n \approx a \left(\frac{Q_\beta - S_n}{Q_\beta - C} \right)^{b+1} \tag{1.11}$$

The cutoff energy, C, represents the pairing gap according to the precursor's odd/even nucleon interaction (McCutchan et al. 2014). A detailed derivation can be found in Madland and Nix (1988):

$$\begin{aligned} C &= 0 && [MeV] && \text{for even-even} \\ C &= 13/\sqrt{A} && [MeV] && \text{for even-odd} \\ C &= 26/\sqrt{A} && [MeV] && \text{for odd-odd} \end{aligned} \tag{1.12}$$

A plot of this fit is shown in Fig. 1.6 using Q_β and S_n values from the mass formula of Garvey et al. (1969). This represented a large improvement on the Amiel-Feldstein systematics.

Since 1969, a wealth of new half-life information and nuclear mass measurements is available, and it is now possible to constrain the systematics further as is shown in McCutchan et al. (McCutchan et al. 2012). The half life can be related to the denominator of Eq. (1.8):

$$\frac{1}{T_{1/2}} \approx \int_0^{Q_\beta} f(Z, Q_\beta - E) S_\beta(E) dE \tag{1.13}$$

Combining Eq. (1.8) with Eq. (1.13) and again assuming the competing gamma decay with neutron emission is negligible gives the result:

$$\frac{P_n}{T_{1/2}} \approx \int_{S_n}^{Q_\beta} f(Z, Q_\beta - E) S_\beta(E) dE \tag{1.14}$$

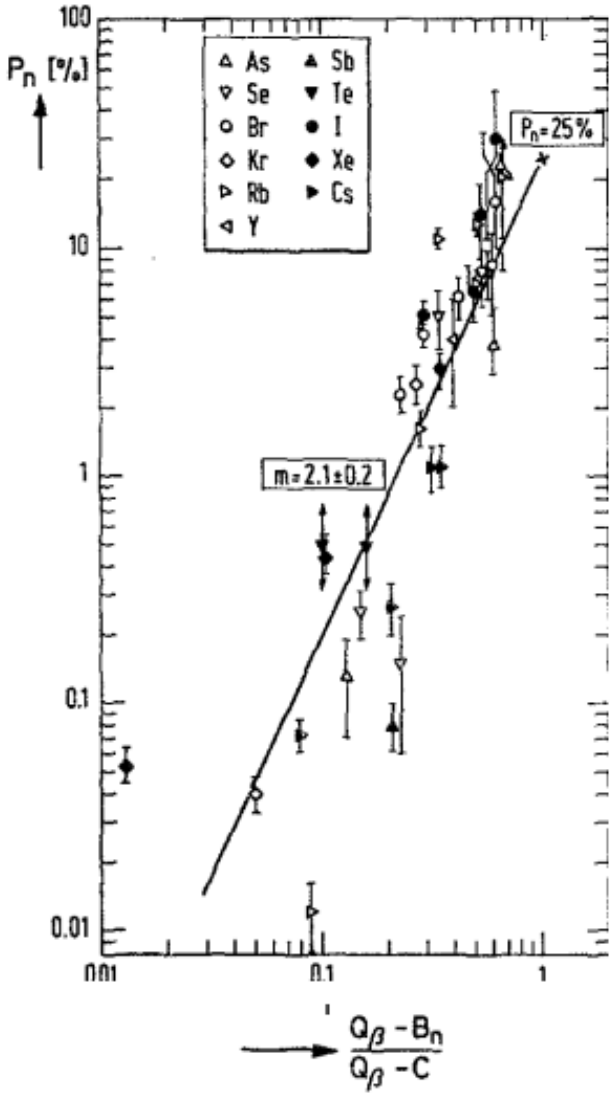

Figure 1.6 Correlation of experimental neutron emission probabilities with energy window using the Kratz-Herrmann Formula and Q_β and E values from the mass formula of Garvey et al. (1969). Figure taken from (Kratz and Herrmann, 1973).

Once again, the β strength function can be approximated as a constant and the integral can be evaluated as a function of the energy window $a(Q_\beta - S_n)^b$ (McCutchan et al. 2012):

$$\frac{P_n}{T_{1/2}} \approx a(Q_\beta - S_n)^b \tag{1.15}$$

In Eqn. 1.15, the variables a and b are fitted to experimental data using a least-squares fit method. A comparison of this method to the Kratz-Herrmann Formula is shown in Fig. 1.7 with Q values calculated from the 2011 update to the Atomic Mass Evaluation work of Audi et al. (AME2012) and P_n values from the 2002 Pfeiffer et al. evaluation for emitters in the Z number 28-43 region.(Pfeiffer et al. 2002)

In the KHF model, the least squares fit using evaluated data from Pfeiffer et al. (2002) yields fitting parameters of a=119(42) and b+1=5.45(48), with a reduced χ^2 of 146. While there is an overall trend, any given value of P_n predicted from $(Q_\beta - S_n)/(Q_\beta - C)$ can span two orders of magnitude. Comparatively, the scatter of the data from the McCutchan method is noticeably more compact, and for a given $Q_{\beta n}$ the scatter is reduced to less than an order of magnitude, with the exception of a few outliers. Additionally, the new fitting parameters a=0.0097 and b=4.87(7) show a χ^2 value of 35 compared to the 146 from the KHF. In addition, the McCutchan et al. systematics succeed in providing a trend to Z<26 with a χ^2 value of 87 compared to the χ^2 value of 280 when fitting with the KHF (McCutchan et al. 2012).

Phenomenological models such as those listed require rigorously compiled and evaluated data. The last evaluation with focus on β-delayed neutron emis-

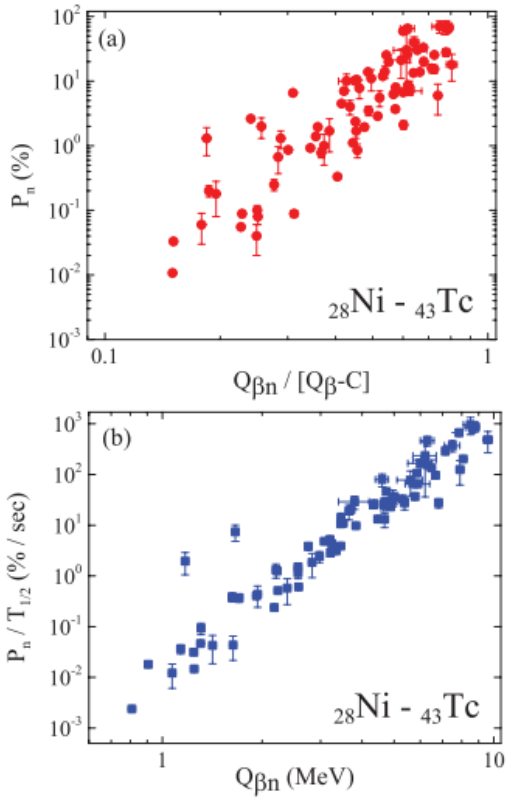

Figure 1.7 Correlation of experimental neutron emission probabilities with energy window using mass evaluations from Audi et al.(2011) and P_n values from 2002 Pfeiffer et al. evaluation with a) Kratz-Herrmann formula and b) systematics from McCutchan et al. Figure from (McCutchan et al. 2012).

sion probability was performed was 14 years ago by Pfeiffer et al.. Since then, a need for this data has arisen, prompting a coordinated research project from the International Atomic Energy Association (IAEA). This project focuses on 3 major aspects: Compilation, evaluation, and systematics of experimental data, theoretical predictions for β-delayed neutron properties, and experimental measurements to complement these predictions. This work focuses mainly on the first of these aspects in the region between $30 \leq Z \leq 40,49,50$, while collaborating groups such as the Chinese Institute of Atomic Energy (CIAE) and the Variable Energy Cyclotron Centre (VECC) have contributed evaluated data for the region between $40 \leq Z \leq 57$. This will act as a continuation of the 2015 evaluation that was completed for $Z \leq 28$ by Birch et al. in 2015.

Chapter 2

Procedure

2.1 β^- Delayed Neutron Emission Compilation and Evaluation

The goal of this thesis is to assess the current state of information on β^--delayed neutron emitters, and identify where better data is required. This is done through a compilation and evaluation of all experimental data for β^--delayed neutron emitters for the Z range $30 \leq Z \leq 40$ and Z=49,50 that exist in literature, so that a single value for P_n and $T_{1/2}$ can be presented per emitter. Approximately 150 nuclides were studied, and over 200 papers were evaluated in this region alone. Aiming to be as comprehensive as possible, there is no cutoff date for the compilation of literature, but outdated measurements are typically eliminated during the evaluation process. The compilation begins by identifying all possible nuclides capable of β^- delayed neutron emission by computing $Q_{\beta n}$ for all nuclides reported in the mass evaluation by Audi et al. (AME2012). All nuclides with positive values of $Q_{\beta n}$ are identified as precursors. Nuclides that are direct neutron emitters ($S_{xn} < 0$, where S_{xn} is

the neutron separation energy for x neutrons) are excluded from this list, thus we exclude isotopes that are close to the neutron dripline. For each identified precursor, experimental data from publications and secondary sources such as theses and laboratory reports concerning half life, $T_{1/2}$, and delayed neutron emission probability, P_n, are compiled.

Each experiment was evaluated based on the method of measurement and how well the results agreed with other experiments. For $T_{1/2}$, the method was typically measurement of neutron activity, β^- particles, or γ rays, with the latter being preferred since it provides many counts. Methods for measuring P_n are as follows:

- n/β coincidence: (Ex:1986WA17) neutrons are measured in coincidence with β particles. The number of coincident neutrons is then compared against the total count of β particles:

  $$P_n = 1/\epsilon_n * N_{\beta n}/N_\beta$$

  where ϵ_n is the efficiency of the neutron detector. This method has the advantage of not requiring the β efficiency since the efficiency term from the coincidence measurement and the total beta measurement will cancel.

- n-β counting: (Ex. 1980LU04) Neutrons and beta particles are counted separately and compared:

  $$P_n = \epsilon_\beta/\epsilon_n * N_n/N_\beta$$

- $\gamma -$ ^{A+1}Z counting: (No example) neutron fraction is determined and compared to the absolute γ-activity of the longer lived daughter. This

method is reserved for β^--decay daughters with sufficiently long half lives compared to the half life of the mother to reduce contamination.

$$P_n = (N_n/\epsilon_n) * \left(\epsilon_\gamma * \frac{I_{abs,\gamma}(^{A+1}Z)}{N_\gamma(^{A+1}Z)}\right)$$

- Fission yields: (Ex. 1949SU14) Isotopes from fission are separated chemically, then any neutron activity is compared to typical fission yields for the isotope of interest. This is the most unreliable method and is typically not selected for evaluation.

The first two methods are preferred since they are more robust and do not rely as heavily on detector efficiencies. Only the selected values are taken into account when recommending a final value. Once a set of measurements is obtained, a weighted average of the values is taken, giving a single recommended value. A table containing the values of Z=30-40,49,50 is given in Table. 3.1. The references given in Table. 3.1 correspond to keynumbers given in the Nuclear Science References (NSR) from the National Nuclear Data Center (NNDC). If the values of the set are discrepant, other averaging methods may need to be used such as the Normalized Residual Method (NRM) (M. James et al. 1992) or simply an unweighted average.

Chapter 3

Results

3.1 β^- Delayed Neutron Emission Compilation and Evaluation

The recommended values for half life, $T_{1/2}$, and x-neutron emission, P_{xn}, are shown in Table 3.1 . Isomers are considered, with n asterisks(*,**) to label the *nth* excited state or (HSPIN), (LSPIN) to label spin states that have unclear ground state spins. The comments should be intepreted as:

WA:[refs] Recommended value was obtained using a weighted average

NRM:[refs] Recommended value was obtained using the normalized residual method (used for discrepant cases)

UWA:[refs] Recommended value was obtained using an unweighted average (used for discrepant cases)

BM:[refs] Recommended value is from the single reference since it is the best available measurement

BM#:[refs] Recommended value is from the single reference since it is the best available measurement' however it was only preliminary

OM:[ref] Recommended value is the single reference since it is the only available measurement

OM#:[ref] Recommended value is the single reference since it is the only available measurement; however it was only preliminary

ID:[ref] Isotope is identified in the reference; however values have yet to be measured

Table 3.1: Recommended Values using best values at time of writing

Nuclide	**$T_{1/2}$ (ms)**	**$\%P_{1n}$**	**$\%P_{2n}$**	**$\%P_{3n}$**	**$T_{1/2}$ Comm.**	**P_n Comm.**
Zinc						
^{78}Zn	1.47(15)	-			OM: 1980WO08	
^{79}Zn	0.914(84)	1.37(40)			UWA: 1986EK01, 1991KR15, 2012HO12	WA: 1991KR15, 2012HO12
^{80}Zn	0.56220(30)	1.0(5)			WA: 1986GI07, 1986EK01, 1991KR15, 2010HO12, 2014XU07	OM: 1991KR15
^{81}Zn	0.3035(30)	30(13)	-		WA: 1991KR15, 2007VE08, 2010PA33, 2010HO12, 2014XU07	OM: 2012HO12
^{82}Zn	0.228(10)	-	-		OM: 2012MA37	

Continued on next page

Table 3.1 – continued from previous page

Nuclide	$T_{1/2}$ (ms)	$\%P_{1n}$	$\%P_{2n}$	$\%P_{3n}$	$T_{1/2}$ Comm.	P_n Comm.
^{83}Zn	0.117(20)	-	-		OM: 2012MA37	—
^{84}Zn	-	-	-		—	—
Gallium						
^{79}Ga	2.8479(49)	0.1048(10)			WA: 1974GR29, 1991KR15, 1993RU01	WA: 1980LU04, 1993RU01
^{80}Ga	1.9(1)	0.846(73)			BM: 2013VE03	NRM: 1984LU06, 1986WA17, 1993RU01
^{81}Ga	1.217(5)	11.8(8)			WA: 1986WA17, 1991KR15, 1993RU01	WA: 1980Lu04, 1986WA17, 1993RU01

Continued on next page

Table 3.1 – continued from previous page

Nuclide	$T_{1/2}$ (ms)	$\%P_{1n}$	$\%P_{2n}$	$\%P_{3n}$	$T_{1/2}$ Comm.	P_n Comm.
^{82}Ga	0.599(2)	31.4(44)			WA: 1986WA17, 1991KR15, 1993RU01, 2012HO12, 2015ET01	
^{83}Ga	0.30798(99)	62.8(25)			WA: 1991KR15, 1993RU01, 2003PE18	OM: 2009WI03
^{84}Ga	0.0848(100)	72(14)	-		WA: 1991KR15, 2009LEZZ, 2010WI03	WA: 1991KR15, 2010WI03
^{85}Ga	0.092(4)	-	-		OM: 2013MI19	
^{86}Ga	$0.043\binom{+21}{-15}$	60(10)	20(10)		OM: 2013MI19	P_{1n} – OM: 2013MI19; P_{2n} – OM: 2013MI19
^{87}Ga	$0.0264\binom{+169}{-110}$	-	-		OM#: 2014XUZZ	

Continued on next page

Table 3.1 – continued from previous page

Nuclide	$T_{1/2}$ (ms)	$\%P_{1n}$	$\%P_{2n}$	$\%P_{3n}$	$T_{1/2}$ Comm.	P_n Comm.
Germanium						
^{83}Ge	1.85(6)	-			OM: 1988WI17	—
^{84}Ge	0.952(11)	10.8(6)			WA: 1991Kr15, 1991OM01, 1993RU01, 2013MA22	OM: 1993RU01
^{85}Ge	0.503(18)	17.2(18)	-		BM: 2013MA22	BM#: 2014AG12
^{86}Ge	0.226(21)	45(15)			OM: 2013MA22	OM: 2013MI19
^{87}Ge	0.1032(35)	-	-		OM#: 2014XuZZ	—
^{88}Ge	0.0608(61)	-	-		OM#: 2014XuZZ	—
^{89}Ge	-	-	-	-	ID: 1997Be12/1997Be~~70~~	
^{90}Ge	-	-	-	-	ID: 2010Oh02	—
Arsenic						

Continued on next page

Table 3.1 – continued from previous page

Nuclide	$T_{1/2}$ (ms)	$\%P_{1n}$	$\%P_{2n}$	$\%P_{3n}$	$T_{1/2}$ Comm.	P_n Comm.
^{84}As	4.18(23)	0.281(38)			NRM: 1991HO10, 1993RU01	BM: 1993RU01
^{85}As	2.02(1)	62.5(10)			WA: 1967DE01, 1991KR15, 1993RU01, 2013MA22	WA: 1991KR15, 1993RU01, 2014AG12
^{86}As	0.944(10)	35.4(6)	-		WA: 1993RU01, 2013MA22	WA: 1993RU01, 2014AG12
^{87}As	0.484(35)	15.4(22)	-		BM: 2013Ma22	BM: 1993Ru01
^{88}As	$0.20\binom{+20}{-9}$	-	-		OM: 2013Ma22	
^{89}As	-	-	-		ID: 1994Be24	
^{90}As	-	-	-		ID: 1997Be70	
^{91}As	-	-	-		ID: 1997Be70	
^{92}As	-	-	-		ID: 1997Be70	
Selenium						

Continued on next page

Table 3.1 – continued from previous page

Nuclide	$T_{1/2}$ (ms)	$\%P_{1n}$	$\%P_{2n}$	$\%P_{3n}$	$T_{1/2}$ Comm.	P_n Comm.
^{86}Se	14.38(13)	-			WA: 1970SA05, 1973TA19, 1974KRZG, 1975HU02, 1977PF01, 1978ZE08	—
^{87}Se	5.51(11)	0.60(12)			WA: 1970KR05, 1970DE08, 1971TO13, 1975HU02, 1978ZE08, 1993RU01	OM: 1993RU01
^{88}Se	1.517(40)	0.99(10)[a]			WA: 1971TO13, 1978ZE08, 1992RE08	BM: 1971To13
^{89}Se	0.440(60)	7.8(25)[b]			WA: 1971TO13, 1982RE08	BM: 1971To13

Continued on next page

Table 3.1 – continued from previous page

Nuclide	$T_{1/2}$ (ms)	$\%P_{1n}$	$\%P_{2n}$	$\%P_{3n}$	$T_{1/2}$ Comm.	P_n Comm.
^{90}Se	0.195(7)	-	-		OM: 2012QU01	—
^{91}Se	0.27(5)	21(10)	-		OM: 1975AS04	OM: 1975AS04
^{92}Se	-	-	-		ID: 1997Be70	—
^{93}Se	-	-	-		ID: 1997Be70	—
^{94}Se	-	-	-		ID: 1997Be70	—
^{95}Se	-	-	-	-	ID: 2010Oh02	—
Bromine						

Continued on next page

Table 3.1 – continued from previous page

Nuclide	$T_{1/2}$ (ms)	$\%P_{1n}$	$\%P_{2n}$	$\%P_{3n}$	$T_{1/2}$ Comm.	P_n Comm.
^{87}Br	55.69(15)	2.59(5)			WA: 1949SU14, 1966SI09, 1966Wi18, 1971DE35, 1974GR29, 1974KR21, 1993RU01	WA: 1964AR24, 1967GA19, 1967PA26, 1971DE35, 1972SC48, 1975IZ03, 1978KR15, 1980LU04, 1980REZQ, 1993RU01
^{88}Br	16.34(8)	6.58(18)			BM: 1993RU01	OM: 1993RU01

Continued on next page

Table 3.1 – continued from previous page

Nuclide	$T_{1/2}$ (ms)	$\%P_{1n}$	$\%P_{2n}$	$\%P_{3n}$	$T_{1/2}$ Comm.	P_n Comm.
^{89}Br	4.36(3)	13.7(6)			WA: 1974NOZR, 1974KR21, 1974GR29, 1976RU01, 1984EW01, 1993RU01	WA: 1972SC48, 1974KR21, 1993RU01, 1978KR15, 1980REZQ, 1980LU04, 1980AL15, 1984EW01, 1987PFZX, 1993RU01
^{90}Br	1.91(1)	26.3(21)			WA: 1975AS04, 1987PFZX, 1993RU01, 2012QU01	WA: 1975AS04, 1987PFZX, 1993RU01
^{91}Br	0.543(11)	29.4(5)			WA: 1975AS04, 1988KR10, 1993RU01, 2012QU01	WA: 1975AS04, 1988KR10, 1993RU01, 2014AG12

Continued on next page

Table 3.1 – continued from previous page

Nuclide	$T_{1/2}$ (ms)	$\%P_{1n}$	$\%P_{2n}$	$\%P_{3n}$	$T_{1/2}$ Comm.	P_n Comm.
^{92}Br	0.310(10)	32.0(45)	-		WA: 1988KR10, 2012QU01	OM: 1988KR10
^{93}Br	0.152(8)	10(5,-3)	-		BM: 2013MI13	OM: 1988KR10
^{94}Br	0.70(20)	30(10)	-		OM: 1988KR10	OM: 1988KR10
^{95}Br	-	-	-		ID: 1997Be70	—
^{96}Br	-	-	-		ID: 1997Be70	—
^{97}Br	-	-	-		ID: 1997Be70	—
^{98}Br	-	-	-		ID: 2010Oh02	—
Krypton Values						
^{91}Kr		-				
^{92}Kr	1.86(1)	0.0332(25)			WA: 1969CA03, 1970LU05, 1976AS05	

Continued on next page

Table 3.1 – continued from previous page

Nuclide	$T_{1/2}$ (ms)	$\%P_{1n}$	$\%P_{2n}$	$\%P_{3n}$	$T_{1/2}$ Comm.	P_n Comm.
^{93}Kr	1.287(12)	1.95(14)			WA: 1969TA04, 1969CA03, 1972AM01, 1975AS04, 2013MI13	WA: 1969TA04, 1975AS04, 2013MI13
^{94}Kr	0.2144(73)	1.11(15)			WA: 2003BE05, 2012QU01, 2013MI13	WA: 2003BE05, 1975AS04
^{95}Kr	0.114(3)	2.87(18)	-		BM: 2003BE05	BM: 2003BE05
^{96}Kr	0.080(7)	3.7(4)			BM: 2003BE05	BM: 2003BE05
^{97}Kr	0.063(4)	6.7(6)	-		BM: 2003BE05	BM: 2003BE05
^{98}Kr	0.046(8)	7.0(10)	-		BM: 2003BE05	BM: 2003BE05
^{99}Kr	0.040(11)	11(7)	-		BM: 2003BE05	
^{100}Kr	$0.07\binom{+11}{-3}$	-	-		OM: 2011NI01	
^{101}Kr	-	-	-	-	ID: 2010Oh02	—

Continued on next page

Table 3.1 – continued from previous page

Nuclide	$T_{1/2}$ (ms)	$\%P_{1n}$	$\%P_{2n}$	$\%P_{3n}$	$T_{1/2}$ Comm.	P_n Comm.
Rubidium						
^{91}Rb	57.9(2)				WA: 1967AM01, 1969CA03, 1970CHYZ, 1974GR29, 1974AC01	
^{92}Rb	4.50(2)	0.0109(7)			WA: 1969TA04, 1969CA03, 1977RE05, 1979EN02, 1993RU01	WA: 1969TA04, 1969CA03, 1977RE05, 1979EN02, 1993RU01
^{93}Rb	5.85(3)	1.44(8)			WA: 1969TA04, 1969CA03, 1972AM01, 1975AS04, 1981EN05, 1993RU01	WA: 1969TA04, 1974RO15, 1975AS04, 1980REZQ, 1980LU04, 1981EN04, 1993RU01

Continued on next page

Table 3.1 – continued from previous page

Nuclide	$T_{1/2}$ (ms)	$\%P_{1n}$	$\%P_{2n}$	$\%P_{3n}$	$T_{1/2}$ Comm.	P_n Comm.
^{94}Rb	2.72(2)	10.3(3)			WA: 1974RO15, 1975AS04, 1979RI09, 1981EN05, 1993RU01	WA: 1974RO15, 1975AS04, 1979WAZU, 1979RI09, 1981EN05, 1986OK07, 1993RU01, 2011GO37
^{95}Rb	0.3912(59)	9.00(11)			UWA: 1974RO15, 1975BA36, 1979RI09, 1981EN05, 1986REZS, 1993RU01, 2012QU01	WA: 1975RO15, 1979RI09, 1981EN05, 1986OK07, 1986REZS, 1993RU01

Continued on next page

Table 3.1 – continued from previous page

Nuclide	$T_{1/2}$ (ms)	$\%P_{1n}$	$\%P_{2n}$	$\%P_{3n}$	$T_{1/2}$ Comm.	P_n Comm.
^{96}Rb	0.2109(11)	13.8(8)			WA: 1971TR02, 1977RE05, 1978WO09, 1979RI09, 1981EN05, 1993RU01, 2012QU01	WA: 1979RI09, 1980REZQ, 1981EN05, 1993RU01, 2012QU01
^{97}Rb	0.169(1)	25.6(11)			WA: 1974RO15, 1978WO09, 1979RI09, 1979PE01, 1979EN02, 1981EN05, 1986WA17, 1987PFZX, 1993RU01, 2011NI01, 2012QU01	WA: 1980REZQ, 1981EN05, 1986WA17, 1987PFZX, 1993RU01

Continued on next page

Table 3.1 – continued from previous page

Nuclide	$T_{1/2}$ (ms)	$\%P_{1n}$	$\%P_{2n}$	$\%P_{3n}$	$T_{1/2}$ Comm.	P_n Comm.
^{98}Rb	0.1106(14)	13.5(5)	0.060(9)		WA: 1974RO15, 1976AMZV, 1978WO09, 1979RI09, 1979PE01, 1981EN05, 1983LY06, 1986WA17, 1987PFZX, 1993RU01, 2011NI01	P_{1n} – WA: 1983LY06, 1986WA17, 1987PFZX; P_{2n} – BM: 1981RE05

Continued on next page

Table 3.1 – continued from previous page

Nuclide	$T_{1/2}$ (ms)	$\%P_{1n}$	$\%P_{2n}$	$\%P_{3n}$	$T_{1/2}$ Comm.	P_n Comm.
^{99}Rb	0.564(12)	15.8(24)			NRM: 1993RU01, 1987PFZX	NRM: 1978KO29, 1979PE01, 1983WO10, 1984PF01, 1983RE10, 1986REZU, 1993RU01, 2011NI01, 1993RU01, 1987PFZX
^{100}Rb	0.051(2)	6(3)	0.027(7)		WA: 1978KO29, 1979PE01, 1986WA17, 1987PFZX, 2011NI01	P_{1n} – WA: 1986WA17, 1987PFZX; P_{2n} – OM: 1981JOZV
^{101}Rb	$0.0314\binom{+50}{-40}$	32			WA: 1987PFZX, 2011NI01	OM#: 2010MAZS

Continued on next page

Table 3.1 – continued from previous page

Nuclide	$T_{1/2}$ (ms)	$\%P_{1n}$	$\%P_{2n}$	$\%P_{3n}$	$T_{1/2}$ Comm.	P_n Comm.
^{102}Rb	0.0362(100)				WA: 2011NI01, 2015LO04	
^{103}Rb	$0.023\binom{+13}{-9}$				OM: 2015LO04	
Strontium Values						
^{96}Sr	1.07(1)	-			WA: 1978WO09, 2012QU01	
^{97}Sr	0.431(5)	0.0052(5)			WA: 2012QU01, 1987PFZX, 1986WA17, 1982GA24, 1981EN05, 1978WO09	WA: 1982GA24, 1987PFZX
^{98}Sr	0.653(2)	0.234(23)			BM: 1986REZU	OM: 1993RU01

Continued on next page

Table 3.1 – continued from previous page

Nuclide	$T_{1/2}$ (ms)	$\%P_{1n}$	$\%P_{2n}$	$\%P_{3n}$	$T_{1/2}$ Comm.	P_n Comm.
^{99}Sr	0.269(2)	0.096(11)			BM: 1986REZU	WA: 1982GA24, 1986WA17, 1987PFZX
^{100}Sr	0.202(2)	1.48(12)			WA: 1983MU19, 1986WA17, 1987PFZX, 1987WO07, 1993RU01, 2011NI01	BM: 1993RU01
^{101}Sr	0.113(2)	2.38(14)			WA: 1983WO10, 1986HI02, 1986WA17, 2011NI01	WA: 1986WA17, 1987PFZX
^{102}Sr	0.072(8)	5.4(20)			WA: 1986WA17, 1986HI02, 1987PFZX, 2011NI01	WA: 1986WA17, 1987PFZX

Continued on next page

Table 3.1 – continued from previous page

Nuclide	$T_{1/2}$ (ms)	$\%P_{1n}$	$\%P_{2n}$	$\%P_{3n}$	$T_{1/2}$ Comm.	P_n Comm.
^{103}Sr	0.054(10)	-	-		WA: 2015LO04, 2011NI01	
^{104}Sr	0.050(5)	-	-		WA: 2015LO04, 2011NI01	
^{105}Sr	0.039(5)	-	-		WA: 2015LO04, 2011NI01	
^{106}Sr	$0.020\binom{+8}{-7}$		-		OM: 2015LO04	
^{107}Sr	-	-	-	-	ID: 2010Oh02	—
Yttrium Values						
^{97}Y	3.72(10)	-			NRM: 1981EN05, 1986WA17, 1987PFZX, 1981EN05, 1986WA17	

Continued on next page

Table 3.1 – continued from previous page

Nuclide	$T_{1/2}$ (ms)	$\%P_{1n}$	$\%P_{2n}$	$\%P_{3n}$	$T_{1/2}$ Comm.	P_n Comm.
^{97}Y*	1.16(3)	0.11(3)			WA: 1970EI05, 1976MOZJ, 1986WA17	OM: 1983RE10
^{97}Y**	0.138(15)	-			OM: 1987BO15	
^{98}Y	0.548(2)	0.332(28)			WA: 1977SI05, 1986WA17, 1987PFZX	NRM: 1986WA17, 1987PFZX, 1993RU01, 1986WA17
^{98}Y*	2.03(2)	3.44(95)			WA: 1977SI05, 1981EN05	OM: 1981EN05
^{99}Y	1.477(7)	1.91(40)			WA: 1975AS04, 1979SE01, 1986WA17, 1987PFZX, 1993RU01, 1996ME09, 2012QU01	UWA: 1975AS04, 1986WA17, 1987PFZX, 1993RU01, 1996ME09

Continued on next page

Table 3.1 – continued from previous page

Nuclide	$T_{1/2}$ (ms)	$\%P_{1n}$	$\%P_{2n}$	$\%P_{3n}$	$T_{1/2}$ Comm.	P_n Comm.
^{100}Y	0.727(5)	1.23(30)			NRM: 2012QU01, 2009PE06, 1996ME09, 1993RU01, 1986WA17, 1986WO01, 1985IAZZ, 1983MU19, 1977KH03, 1993RU01	UWA: 1996ME09, 1993RU01, 1986WA17
^{100}Y*	0.94(3)	-			WA: 1977KH03, 1977PF01	
^{101}Y	0.423(20)	1.89(18)			WA: 1983WO10, 1986WA17, 1986REZS, 1986REZU, 1996ME09, 2009PE06	WA: 1986WA17, 1996ME09

Continued on next page

Table 3.1 – continued from previous page

Nuclide	$T_{1/2}$ (ms)	$\%P_{1n}$	$\%P_{2n}$	$\%P_{3n}$	$T_{1/2}$ Comm.	P_n Comm.
^{102}Y(HSPIN)	0.396(36)	5.36(85)			WA: 1983SH13, 1986WA17, 2009PE06	WA: 1986WA17, 1996ME09, 2009PE06
^{102}Y(LSPIN)	0.30(1)	5.36(85)			WA: 1996ME09, 1991HI02	WA: 1986WA17, 1996ME09, 2009PE06
^{103}Y	$0.232\binom{+18,}{-15}$	8.29(3)			WA: 2011NI01, 1996ME09	WA: 2009PE06, 1996ME09
^{104}Y	0.197(4)	34(10)	-		WA: 2015LO04, 2011NI01, 2009PE06, 1999WA09	OM: 2009PE06
^{105}Y	0.097(9)	-	-		NRM: 2009PE06, 2011NI01, 2015LO04, 2011NI01	

Continued on next page

Table 3.1 – continued from previous page

Nuclide	$T_{1/2}$ (ms)	$\%P_{1n}$	$\%P_{2n}$	$\%P_{3n}$	$T_{1/2}$ Comm.	P_n Comm.
^{106}Y	$0.079\binom{+10}{-5}$	-	-		WA: 2015LO04, 2011NI01	
^{107}Y	0.0339(30)	-	-		WA: 2015LO04, 2011NI01	
^{108}Y	0.030(5)	-	-		WA: 2015LO04, 2011NI01	
^{109}Y	0.025(5)	-	-	-	OM: 2015LO04	
Zirconium						
^{103}Zr	1.380(72)	-	-		OM: 2009PE06	
^{104}Zr	0.920(28)	-	-		OM: 2009PE07	
^{105}Zr	0.667(28)	-	-		WA: 1992AY02, 1996ME09, 2009PE06	
^{106}Zr	0.175(7)	-	-		BM: 2015LO04	

Continued on next page

Table 3.1 – continued from previous page

Nuclide	$T_{1/2}$ (ms)	$\%P_{1n}$	$\%P_{2n}$	$\%P_{3n}$	$T_{1/2}$ Comm.	P_n Comm.
^{107}Zr	1.457(41)	-	-		WA: 2009PE06, 2011NI01, 2015LO04	
^{108}Zr	0.0785(3)	-	-		WA: 2011NI01, 2015LO04	
^{109}Zr	0.0561(3)	-	-		WA: 2011NI01, 2015LO04	
^{110}Zr	0.0375(20)	-			WA: 2011NI01, 2015LO04	
^{111}Zr	0.0240(5)	-	-		OM: 2011NI01	
^{112}Zr	$0.030\binom{+30}{-10}$	-	-		OM: 2011NI02	
Tin						
^{133}Sn	1.423(58)	0.0294(24)			NRM: 1973BO43, 1978SI05, 1993RU01	OM: 1993RU01

Continued on next page

Table 3.1 – continued from previous page

Nuclide	$T_{1/2}$ (ms)	$\%P_{1n}$	$\%P_{2n}$	$\%P_{3n}$	$T_{1/2}$ Comm.	P_n Comm.
^{134}Sn	1.048(20)	17(13)			NRM: 1990FO03, 1993RU01, 2015LO04	WA: 1975AS04
^{135}Sn	0.515(5)	21(3)			WA: 2001KO45, 2002SH08, 2015LO04	OM: 2002SH08
^{136}Sn	0.350(5)	27(4)			BM: 2015LO04	BM: 2011AR18
^{137}Sn	0.271(10)	50(10)			WA: 2011AR18, 2015LO04	OM: 2011AR18
^{138}Sn	$0.140\binom{+30}{-20}$				OM: 2015LO03	
^{139}Sn	0.130(60)				OM: 2015LO04	
Indium						

Continued on next page

Table 3.1 – continued from previous page

Nuclide	$T_{1/2}$ (ms)	$\%P_{1n}$	$\%P_{2n}$	$\%P_{3n}$	$T_{1/2}$ Comm.	P_n Comm.
^{127}In	1.09(9)	<0.03			WA: 1974Gr29, 1980DE35, 1983SH07, 1986GO07, 1993RU01	BM: 1993RU01
^{127}In*	3.618(32)	0.699(58)			WA: 1974Gr29, 1983SH07, 1986WA17, 1993RU01	WA: 1986WA17, 1993RU01
^{128}In	0.80(1)	0.0384(36)			BM: 1986WA17	WA: 1986WA17, 1993RU01
^{128}In*	0.72(10)				OM: 1986GO10	
^{129}In	0.609(7)	0.331(32)			NRM: 1986WA17, 1986GO10, 1993RU01, 2015LO04	BM: 1993RU01
^{129}In*	2.52(52)	3.92(19)			BM: 1986WA17	BM: 1993RU01

Continued on next page

Table 3.1 – continued from previous page

Nuclide	$T_{1/2}$ (ms)	$\%P_{1n}$	$\%P_{2n}$	$\%P_{3n}$	$T_{1/2}$ Comm.	P_n Comm.
^{130}In	0.287(13)	1.49(22)			WA: 1981FO02, 1986WA17, 1993RU01, 2015LO04	BM: 1993RU01
^{130}In*	0.541(9)	1.87(16)			WA: 1981FO02, 1981EN05, 1983SH07, 1986WA17, 1993RU01	NRM: 1981EN05, 1986WA17, 1993RU01
^{131}In	0.277(3)	2.64(13)			NRM: 1981EN05, 1983SH07, 1984FO19, 1986WA17, 1993RU01, 2015LO04, 2015LO04, 1993RU01	BM: 1993RU01
^{131}In*	0.28(3)				OM: 1984FO19	

Continued on next page

Table 3.1 – continued from previous page

Nuclide	$T_{1/2}$ (ms)	$\%P_{1n}$	$\%P_{2n}$	$\%P_{3n}$	$T_{1/2}$ Comm.	P_n Comm.
$^{131}In^{**}$	0.32	<0.1			OM: 1984FO19	OM: 1984FO19
^{132}In	0.200(2)	6.89(58)			WA: 1980LU04, 1986BJ01, 1986WA17, 1993RU01, 2002DI12, 2015LO04	
^{133}In	0.165(3)	85(10)			WA: 1996HO16, 2002DI12, 2015LO04	OM: 1996HO16
^{134}In	0.136(5)				WA: 1996HO16, 2002DI12, 2015LO04	
^{135}In	0.101(5)				WA: 2002DI12, 2015LO04	
^{136}In	$0.086\binom{+10}{-8}$				OM: 2015LO04	

Continued on next page

Table 3.1 – continued from previous page

Nuclide	$T_{1/2}$ (ms)	$\%P_{1n}$	$\%P_{2n}$	$\%P_{3n}$	$T_{1/2}$ Comm.	P_n Comm.
^{137}In	$0.065^{(+40)}_{(-30)}$				OM: 2015LO04	

[a] Value updated using 1993Ru01 fission yields, original: 0.75(6)

[b] Value updated using 1993Ru01 fission yields, original: 5.0(15)

Chapter 4

Discussion

There were many cases of discrepant values for $T_{1/2}$ and P_n as well as some cases which require comment. However, this work is still preliminary and will undergo a more rigorous analysis before those cases are discussed.

4.1 β^- Delayed Neutron Emission

With systematics discussed in Section 1.3, the evaluated data is used to plot systematics curves. The range of nuclides used was Z=30-57, where P_n was available, totalling 136 data points.

Using the McCutchan et al. analysis method, and fitting the data to the equation $P_n/T_{1/2} = a(Q_{\beta n})^b$, a value for the coefficients a and b are determined with $a = 0.0718$ and $b = 3.7218$, and a coefficient of determination R^2 of 0.8322. The χ^2 of this fit was found to be 112. This is compared to the fit to the Kratz-Herrmann equation $P_n/T_{1/2} = a\left(\frac{Q_{\beta n}-S_n}{Q_{\beta n}-C}\right)^n$ which yields a value of $a = 52.663$ and $n = 3.398$, and an R^2 of 0.6918. The χ^2 of this fit was found to be 140. The fit using the McCutchan et al. method is evidently more robust and gives a closer fit when compared to the Kratz-Herrmann formula. With

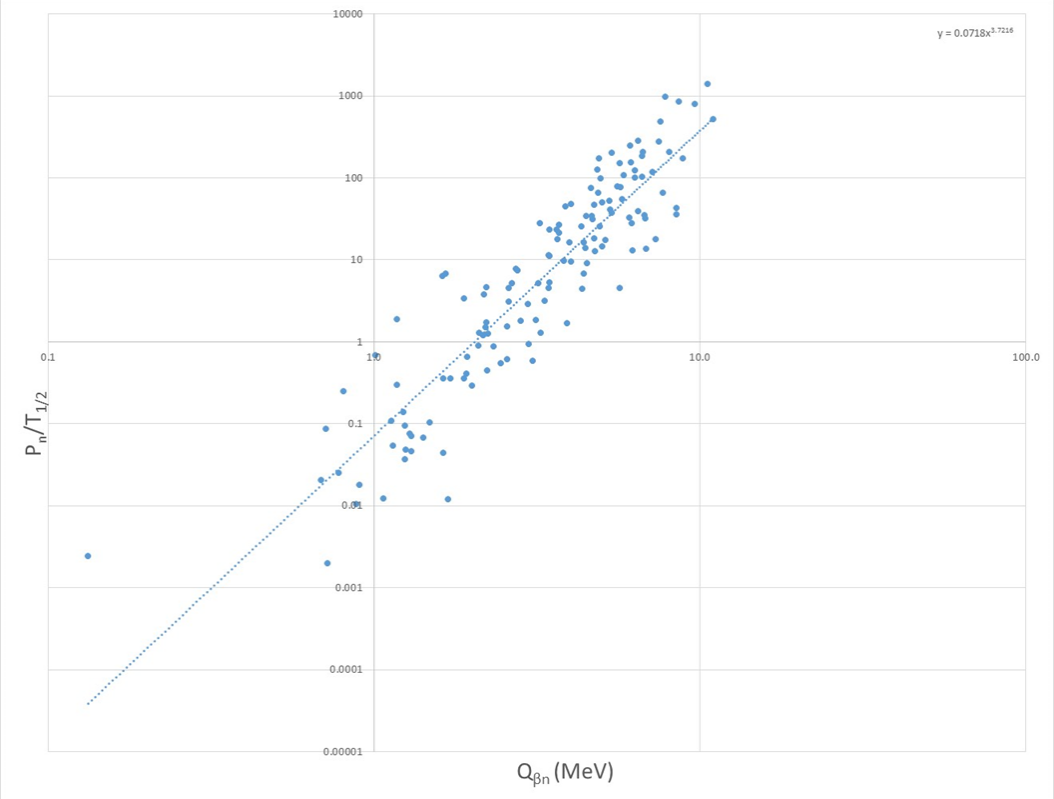

Figure 4.1 β^--delayed neutron emission systematics using formula given by McCutchan et al.: $P_n/T_{1/2} = a(Q_{\beta n})^d$ and range Z=30-57. The variables a and d are fitted to the slope, yielding $a = 0.0718$ and $d = 3.7218$, and a coefficient of determination R^2 of 0.8322.

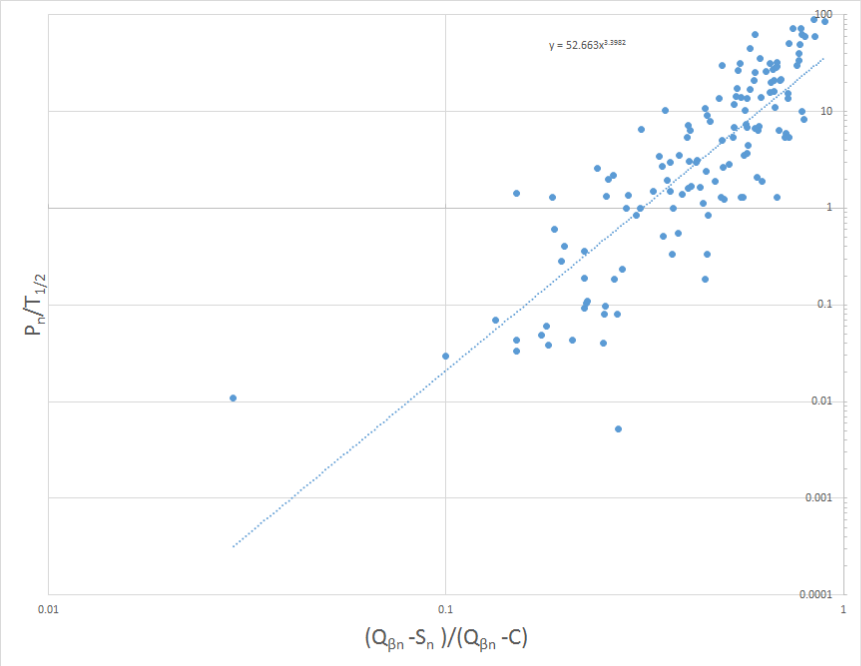

Figure 4.2 β^--delayed neutron emission systematics using formula given by Kratz and Herrmann: $P_n/T_{1/2} = a\left(\frac{Q_{\beta n}-S_n}{Q_{\beta n}-C}\right)^n$. The variables a and b are fitted to the slope, yielding $a = 52.663$ and $n = 3.398$, and a coefficient of determination R^2 of 0.6918. The χ^2 was found to be 140

only a few exceptions, the values of $P_n/T_{1/2}$ fall within a factor of 10 to the fit. Another observation is that at lower Q values, there is a larger deviation from the fit in the KHF method compared to the McCutchan et al. method.

The limitation to using the improved McCutchan et al. systematics is that a half-life is required. When these values are not known from experiment, one can estimate the values using systematics. Pfieffer et al. show that the half life and beta decay Q value are related by:

$$T_{1/2} = a(Q_\beta - C)^b \tag{4.1}$$

where a and b are free parameters that are fitted to data and C is the cutoff parameter described in the Kratz-Herrmann Formula. These systematics are plotted on Fig. (4.3), with fitting parameters of $a = 2747$ and $b = -4.235$ obtained from least squares fitting in the region $30<Z<57$. This is comparable to the values determined by Birch et. al. 2015, of $a = 9549$ and $b = -4.9$ for the region $Z<28$.

In addition, the experimental P_n values were compared to calculated Quasi-particle Random Phase Approximation (QRPA) values for P_n by Möller et. al . Details on this calculation can be found in the 2002 Pfieffer compilation (Pfieffer et. al. 2002). The ratio of theoretical values to evaluated values is plotted in Fig. 4.4. Most evaluated values are within a factor of 10 to the predictions, with a few outliers. Of note are the large deviations at neutron numbers just above the full neutron shells, N=51-55 and N=85-90, corresponding to full shells N=50 and N=82 respectively. At these neutron numbers, the QRPA underestimates the value of P_n when compared to the experimental values.

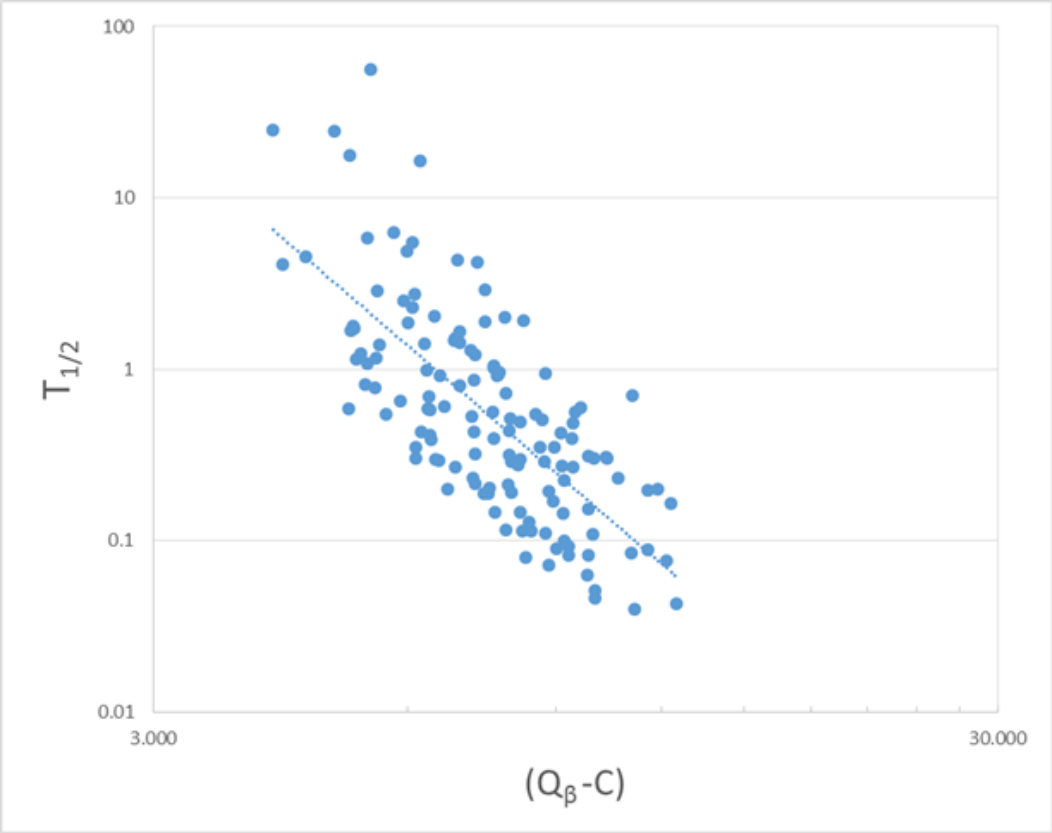

Figure 4.3 $T_{1/2}$ as a function of $(Q_\beta - C)$. Systematic parameters were determined to be $a = 2747$ and $b = -4.235$ using least squares fitting

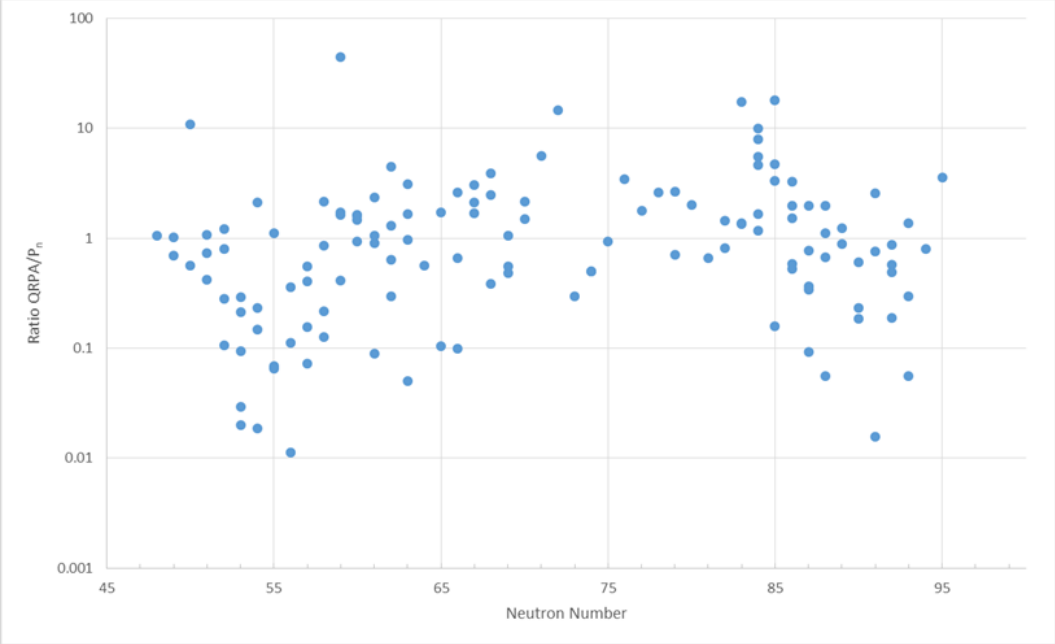

Figure 4.4 A plot of the ratio of theoretical to experimental β^--delayed neutron emission probabilities. Theoretical values were produced from QRPA calculations. Evaluated data was used for the experimental numbers.

Chapter 5

Introduction: Sensitivity Study for Classical Nova Endpoint Nuclei

5.1 Classical Novae

Classical novae are stellar explosions that can occur in close, interacting binary systems between a white dwarf and a companion low-mass-main-sequence star and can produce intermediate-mass nuclei in various abundances up to ^{40}Ca. The entire process begins with a mass transfer episode caused by a Roche lobe overflow of H-rich material from the main sequence star, which proceeds through the inner Lagrangian point of the system (Jose, Hernanz Iliadis, 2006). The material will form an accretion disk around the white dwarf and a fraction of this material will fall inwards towards the surface of the white dwarf. Typical accretion rates for this event range from 10^{-9} - 10^{-10} $M_{\odot}$ per year (Parikh et al. 2014); however this range is still under investigation. The rate at which the white dwarf accretes matter is important, as it affects the characteristics of the nova outburst. The lower the mass accretion rate, the larger the amount of accreted mass can be attained before thermonuclear runaway is intiated. A

more massive layer in turn gives rise to higher pressure in the bottom layer which leads to a more violent explosion (Iliadis, 2015).

The material that spirals in will accumulate and be heated and compressed from the strong surface gravity. The bottom layer of the accumulated layer will eventually become electron degenerate. Fusion of hydrogen occurs, gradually increasing the temperature, but electron degeneracy prevents the expansion of the envelope, which leads to thermonuclear runaway at the base of the accreted layers (Jose, Hernanz, and Iliadis, 2006). Compressionial heating and nuclear burning of the hydrogen fuel through the hot CNO cycle continues until the temperature reaches a point where degeneracy is lifted (Parikh et al. 2014) and a nova ourburst occurs. This event can eject 10^{-5} - 10^{-6} $M_{\odot}$ of material at mean velocities of 10^3 km/s (Iliadis, 2015). Contrary to a Type Ia supernova which fully disrupts the white dwarf with a violent explosion, a classical nova is recurring, with periodicities of 10^4 - 10^5 years. (Parikh et al. 2014)

Isotopic abundances can be determined from observational evidence in the optical, ultraviolet and infrared spectra. In general there is: i) an enhancement of carbon, nitrogen and oxygen in nova ejecta with respect to solar abundances and ii) enrichment of neon in some of them. The first observation suggests that at some point of the evolution of the outburst, carbon and oxygen from the white dwarf was "dredged up" and mixed with the accreted material (Parikh et al. 2014). The second observation cannot be explained with CNO enrichments alone, since temperatures attained during nova outbursts are not capable of producing neon. Thus, some neon must already be present in the white dwarf and is also dredged up into the outburst, leading to the classification of two

white dwarf types that are able to produce Nova explosions: Carbon-oxygen (CO) and oxygen-neon (ONe).

This distinction arises due to differences in mass of the progenitor star: CO white dwarfs have progenitor stars smaller than 9-10$M_{\odot}$, whereas the more masssive ONe white dwarf progenitors are able to undergo non-degnerate carbon ignition which leads to a formation of a degenerate core mainly made of oxygen and neon (Jose, Hernanz and Iliadis 2006). This also plays a role in the peak novae temperatures, as ONe novae can reach higher temperatures (T $\approx$ 0.4 GK), than CO novae (T $\approx$ 0.2 GK) (Lotay et al. 2016). In summary, the nova ejecta characteristics depend on mass and luminosity of the white dwarf, mass accretion rate, and chemical composition of the accreted and white dwarf material (Iliadis, 2015).

The peak temperature of ONe novae is expected to support the production of elements as heavy as Ar and Ca, the theoretical endpoint of novae nucleosynthesis. However, there are very few astronomical studies that show the presence of Ca and Ar in the ejecta of novae; additionally, the amount of Ca and Ar observed in those studies have significant enhancement when compared to solar values, contradicting theoretical models of nova nucleosynthesis.(Lotay et al. 2016).

This motivates the current work, which is a sensitivity study on the reaction rates of isotopes in the classical nova nucleosynthesis pathway. The reaction pathway proceeds to heavier nuclei by (p,γ) reactions and β^{+} decay. In general the pathway traverses the proton-rich side of the table of nuclides. Fig. 5.1

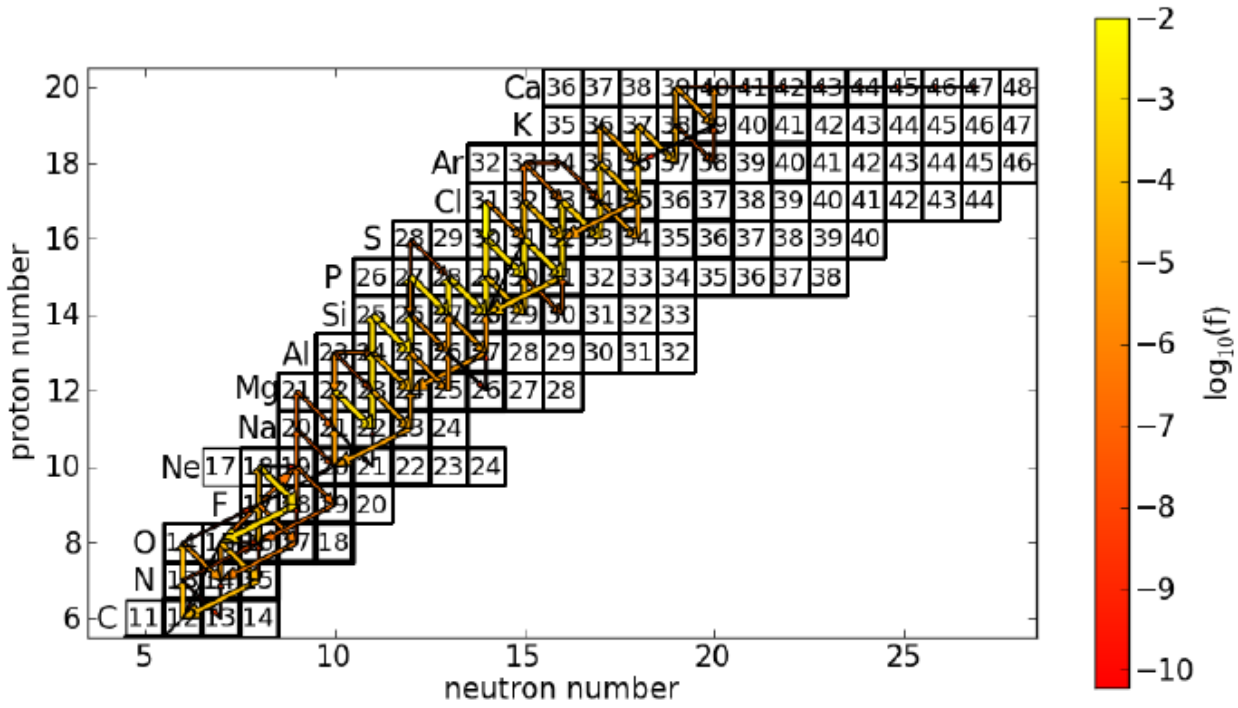

Figure 5.1 Classical Nova reaction pathway for a simulation produced by NuGrid at a moment where T=408 GK (peak temperature used in that simulation). The flux of each reaction is shown, with a colour code to show the intensity. Figure from (Denissenkov et al. 2014).

shows the reaction path for nova nucleosynthesis, eventually reaching the endpoint at ^{40}Ca

The reaction rates and the variables that control them will be discussed in further detail in the next section.

5.2 Thermonuclear Reaction Rates

The reaction rate describes the change in abundance of nuclei as a result of nuclear processes. This quantity is integral to understanding nucleosynthesis in the universe. In astrophysical environments, such as hot plasma consisting of free electrons and ionized atomic nuclei, kinetic energy available to nuclei is that of their thermal motion (Iliadis, 2015). This lends itself to fusion reactions for light nuclei, which in turn produce energy and are responsible for nucleosynthesis in stars and explosive events. Reaction rates are defined mainly by two quantities: the nuclear cross section of the reaction and the relative velocity of the particles.

Consider the reaction $0 + 1 \rightarrow 2 + 3$. The nuclear cross section, σ, is a measure of probability per pair of interacting nuclei 0 and 1 that a nuclear reaction will occur. Nuclear cross sections, in general, will depend on the relative velocity between the particles, that is: $\sigma = \sigma(v)$. One can show that the rate of a nuclear reaction, the number of nuclear reactions per unit time, is

$$r_{01} = N_0 N_1 v \sigma \tag{5.1}$$

where N_0 and N_1 are the number densities of the interacting particles (in units of particles per volume), v is the relative velocity of the interacting nuclei and σv is the reaction rate per particle pair. In a stellar environment, the velocities of the interacting particles can vary. Thus, there is a distribution of relative velocities which can be described by a probability function $\mathrm{P}(v)$. $\mathrm{P}(v)dv$ defines the probability of a particle having velocity in the range $v + dv$. The reaction rate for a distribution of relative velocities can be written as:

$$r_{01} = N_0 N_1 \int_0^\infty v P(v) \sigma(v) dv = N_0 N_1 < \sigma v >_{01} \tag{5.2}$$

with the normalization condition such that

$$\int_0^\infty P(v) dv = 1$$

Since stellar plasma acts as like an ideal gas, $P(v)$ is sufficiently described with a Maxwell-Boltzmann distribution, and it can be expressed as:

$$P(v)dv = \left(\frac{m_{01}}{2\pi kT}\right)^{3/2} [exp\frac{E}{kT}] 4\pi v^2 dv \tag{5.3}$$

Alternatively, with $E = m_{01}v^2/2$, the probability distribution can be rewritten as function of energy

$$P(E)dE = \frac{2}{\sqrt{\pi}} \frac{1}{(kT)^{3/2}} \sqrt{E} e^{-E/kT} dE \tag{5.4}$$

Fig. 5.2 shows examples of Maxwell-Boltzmann probability distributions of various astrophysical scenarios.

Finally, the general expression for the reaction rate can be obtained with Eqn. 5.2 combined with Eqn. 5.4.

$$N_A < \sigma v >_{01} = \left(\frac{8}{\pi m_{01}}\right)^{1/2} \frac{N_A}{(kT)^{3/2}} \int_0^\infty E\sigma(E) e^{-E/kT} dE \tag{5.5}$$

where N_A is Avogadro's number has replaced the number densities of species 1 and 2, m_{01} is the reduced mass, E is the center of mass energy

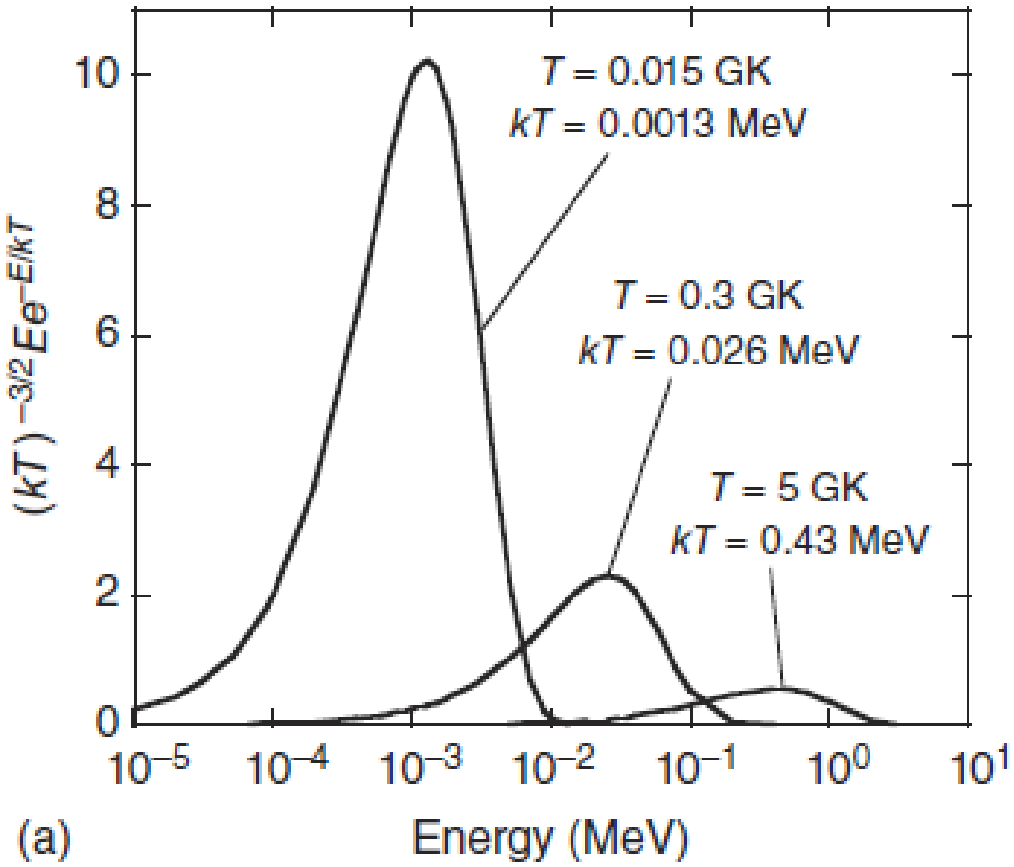

Figure 5.2 The factor$(kT)^{-3/2}Ee^{-E/kT}$ as a function of energy for 3 different temperatures, T=0.015 GK, 0.3GK and 5 GK. These temperatures are found in the Sun, classical novae and type II supernovae respectively. Figure from (Iliadis, 2015).

and is equal to $m_{01}v^2/2$, k is the Boltzmann constant and T is the temperature. How the cross section $\sigma(E)$ varies with energy defines if the reaction will be non-resonant or resonant. In the case of a non-resonant reaction, the cross section varies smoothly with incident kinetic energy and proceeds very quickly. These reactions are generally associated with direct reactions where only the surface nucleons interact and due to the short time frame of interaction, fewer internal collisions are possible (Thompson and Nunes, 2011).

Resonant reactions, however, vary strongly in the vicinity of a particular energy. To understand this, one must explore the details of a resonant reaction. Compared to a non-resonant reaction, the energy of the incident particle is low, and thus its de Broglie wavelength is relatively larger (Setoodehnia, 2011). This means it will interact with the entire nucleus, rather than the surface nucleons. The end result is that in these reactions, the projectile fuses with the target and produces an excited system called the compound nucleus. A compound nucleus can stay in this metastable state for a sufficiently long time so that the excitation energy is redistributed among many nucleons through successive collisions between nucleons (Satchler, 1990). When enough energy has localized on either one or a group of nucleons, they can escape from the compound nucleus, and the new system will subsequently de-excite. This is given schematically as: $0+1 \rightarrow C* \rightarrow 2+3$ where C* is the compound nucleus. An interesting property is that the compound nucleus has quasi-stationary quantum states, or in other words, the compound nucleus exhibits discrete energy states below and above the threshold for particle emission. As a result, there is a higher chance of formation of the compound nucleus if the centre of mass energy in the entrance channel matches the energy of the excited state:

$$Q + E_r = E_x \tag{5.6}$$

where Q is the Q value of the reaction between 0 and 1, E_r is the "resonance energy" and E_x is the excitation energy of a discrete level in the compound nucleus. If the excitation energy of the compound nucleus is below the threshold of particle emission, it is said to be in a "bound state" where it will de-excite via γ decay or β emission. If it has an excitation energy above the threshold, the state is known as a resonance, where particle emission can also occur. Higher resonance energies will open the possibility of heavier particle emissions to de-excite the resonance.

Quantum effects must first be addressed before moving on to the next step. Due to the Heisenberg uncertainty principle, the lifetime of a compound nucleus, τ will play a role in the uncertainty of the excitation energy of that nucleus. Therefore excitation energies will have a gaussian distribution wiith a characteristic width related to the lifetime of that state by:

$$\Gamma = \frac{\hbar}{\tau}. \tag{5.7}$$

Because the cross section increases significantly in the presence of a resonance, the reaction rates at stellar temperatures are dominated by resonant contributions. The reaction can be divided into two steps - formation and decay - and it follows that the cross section should be proportional to the partial widths for formation and decay of the compound state:

$$\sigma \; \alpha \; \Gamma_a \Gamma_b \tag{5.8}$$

where Γ_a and Γ_b are the partial widths of the formation and decay widths respectively. As the resonance energy increases, the width of the resonance increases, as does the density of resonances. For stellar reaction rates in classical novae, isolated and narrow-resonances dominate the reaction rate. The first condition means that the density of levels must be small such that the resonances do not overlap. The second condition is that the resonance must be narrow such that the corresponding partial width and Maxwell-Boltzmann function ($e^{-E/kT}$) is approximately constant over the width. An isolated resonance is well described by the one-level Breit-Wigner formula (Iliadis 2015):

$$\sigma_{BW}(E) = \frac{\lambda^2}{4\pi}\frac{(2J+1)(1+\delta_{01})}{(2j_0+1)(2j_1+1)}\frac{\Gamma_a\Gamma_b}{(E_r-E)^2+\Gamma^2/4} \tag{5.9}$$

where λ is the de Broglie wavelength, j_i are the spins of the target and projectile, J and E_r are the spin and energy of the resonance, Γ_i are the partial resonances of the entrance and exit channel, and γ is the total width. finally the factor $(1+\delta_{01})$ is included since identical particles in the entrance channel increases the cross section by a factor of 2. This cross section can be substituted into Eqn. 5.5

$$N_A < \sigma v >= N_A\frac{\sqrt{2\pi}\hbar^2}{(m_{01}kT)^{3/2}}\omega\int_0^\infty \frac{\Gamma_a\Gamma_b}{(E_r-E)^2+\Gamma^2/4}e^{-E/kT}dE \tag{5.10}$$

where $\omega = (2J+1)(1+\delta_{01})(2j_0+1)(2j_1+1)$. In the assumption of narrow resonances, the partial widths and Maxwell-Boltzmann function are constant over the width, thus they can be replaced by their values at E_r, the resonance energy. After simplification, and rearranging terms to make the integral an-

alytic, the following expression for reaction rates for a narrow resonance is obtained:

$$N_A < \sigma v >= N_A \frac{2\pi}{(m_{01}kT)^{3/2}} \hbar^2 e^{-E_r/kT} \omega\gamma \tag{5.11}$$

where $\gamma = \Gamma_a \Gamma_b / \Gamma$ and the product $\omega\gamma$ is known as the "resonance strength". Thus the reaction rate depends on just 2 experimental parameters: resonance strength and resonance energy. If several narrow and isolated resonances contribute to the cross section, they will add incoherently,

$$N_A < \sigma v >= N_A \frac{2\pi}{(m_{01}kT)^{3/2}} \hbar^2 \sum_i e^{-E_i/kT} \omega\gamma \tag{5.12}$$

A caveat to this equation is that it is for "laboratory" reaction rates. In astrophysical environments, there are myriad coloumbic interactions such as free electrons and ionized particles within the stellar plasma. Luckily, classical nova simulation programs such as MESA and NuGrid can account for these interactions. This equation also assumes that the nuclei are in their ground state when interacting which is not always true.

Chapter 6

Procedure

6.1 Sensitivity Study for Classical Nova Endpoint Nuclides

The goal of this project is to explore the abundances of isotopes in nova ejecta to further our understanding of end-point nucleosynthesis in classical novae. Specifically we want to find which reactions most strongly affect the abundances to motivate additional experimental work. Simulations for novae were performed with the MESA stellar evolution code and the isotopic abundance evolutions were calculated by the post-processing nucleosynthesis code NuGrid. These codes will be expanded upon in the next section. The (p,γ) reaction rates of $^{36-40}$Ar,$^{37-40}$K and $^{39-42}$Ca were varied by a factor of 100 times up and down, one at a time to determine the effect on the final abundances. These variations represent the maximum amount of uncertainty that one would expect from theoretical reaction rates. Two nova conditions were examined:

CO nova:

- White dwarf mass: 1.15 $M_{\odot}$
- Initial central temperature: 10 MK
- Peak temperature: 256MK
- Accretion rate 1x10$^{-11} M_{\odot}/year$

ONe Nova:

- White dwarf mass: 1.3 $M_{\odot}$
- Initial central temperature: 20 MK
- Peak temperature: 315 MK
- Accretion rate: 2x10$^{-10} M_{\odot}/year$

A baseline abundance plot was made with reaction rates as close to nova conditions as possible. These baseline abundances are shown for a CO and ONe nova with conditions outlined in Fig. 7.1 and 7.2. Reaction rates for various (p,γ) reactions were then adjusted by factors of 100 to see the effect on the final abundances, and plotted. The ratio between this new abundance plot and the baseline plot is taken. An example of this can be found in Fig. 8.1 for ^{36}Ar.Finally, the factor of change in the final abundance that each adjustment in reaction rate causes is tabulated. This is shown in tables 7.1 and 7.2.

6.2 MESA and NuGrid

To model classical novae, a combination of two programs are used: MESA and NuGrid. MESA is a collection of Fortran 95 **m**odules for **e**xperiments in **s**tellar **a**strophysics. Its function is to create a simulation of a nova event.

Several Equations of State (EOS) are used to describe the evolution of thermodynamic variables. Pre-existing models that are used are the OPAL EOS tables (Rogers and Nayfonov, 2002) and SCVH EOS (Saumon et al., 1995) for lower temperatures and densities. HELM EOS (Timmes and Swesty 2000) and PC EOS (Potekhin and Chabrier 2010) are also used to cover regions where the first two are not applicable, and account for different physical phenomena; HELM accounts for electron positron pairs at high temperature and PC accounts for crystallization at low temperature. There are smooth transitions between all four of these EOS tables when computing nova evolution parameters

To model the energy generation, a nuclear network of isotopes and reactions is needed. The network must strike a balance between being extensive enough to accurately model the event, but small enough so that the simulations can be done within a reasonable time frame. A large network was used at first, with 77 isotopes from H to ^{40}Ca coupled with 442 reactions, and gradually, reactions and isotopes that did not have significant effect on the peak temperature were eliminated. For CO nova simulations, this reduced the number of isotopes of interest to 33, coupled to 65 reactions. For ONe nova simulations, the number of isotopes used were 48, coupled by 120 reactions. A list of these isotopes can

be found in Denissenkov et al. (Denissenkov et al. 2013). These reactions were typically relevant to the p-p chains, CNO cycle, and NeNa cycles.

Reaction rates were taken from Caughlan and Fowler 1988 (Caughlan and Fowler 1988) and Angulo et al.1999 (Angulo et al. 1999) with preference to the second source.

The mixing of white dwarf material and the accreted material must also be modeled. For this there are 3 approaches:

First type: Neglect boundary mixing and assume that the white dwarf accretes solar-composition matter. These models are not accurate since they do not show the fast rise time or heavy element enrichments that are observed.

Second type: Assume that the accreted matter has solar composition and that it is mixed with white dwarf material before and during the thermonuclear runaway. A possible mechanism for this mixing is through hydrodynamic instabilities and shear flow turbulence induced by steep horizontal velocity gradients in the bottom of the convection zone triggered by thermonuclear runaway. This leads to convective boundary mixing (CBM) and white dwarf material (which is CO-rich for CO novae, and ONe-rich for ONe novae) is dredged up during runaway.This time dependent CBM can be modeled as a diffusion process with an exponentially decreasing function of distance with a formal convective boundary (Denissenkov et al. 2013)

$$D_{CBM} = D_0 exp\left(-\frac{2|r - r_0|}{f H_p}\right) \tag{6.1}$$

where H_p is the pressure scale height, D_0 is a diffusion coefficient, calculated using mixing length theory that describes convective mixing at a radius r_0 close to the boundary. f is a free parameter which was determined to be $f = 0.004$ from fitting heavy element abundances from the simulation to multi-dimensional hydrodynamic simulations and spectroscopic measurements of abundances in nova ejecta (Denissenkov et al. 2013).

Third type: The CBM is neglected is artificially obtained by assuming the white dwarf accretes a mixture which is already blended with some amount of WD material. The amount of material in the mixture can vary from 25-75 % to match observed values. The initial pre-mixed abundances come from the isotope abundances of the outermost layers of the naked ONe white dwarf model.

MESA uses the third type, which is generally used for 1-D nova simulations because it is not as computationally intensive as the second model, and provides comparably accurate results. The temperature trajectory, that is the evolution of maximum temperature over time, and the corresponding density profiles can be used by NuGrid to trace nucelosynthesis. The caveat to this method is that it does not take into account abundance changes occuring in other parts of the nova envelope due to convective mixing.

To reiterate, the MESA code simulates the progression of the nova and only the most relevant isotopes and reactions to achieve accuracy are used in order to reduce computation time. The NuGrid Single-zone Post-Processing Nucleosynthesis (SPPN) code is used to study nucleosynthesis in more detail given the stellar structure models prepared by MESA as an input. The NuGrid

nuclear network contains more than 5000 isotopes coupled by more than 50000 reactions. In that network, a list of 147 isotopes coupled by more than 1700 reactions are relevant for nova nucleosynthesis simulations.

Chapter 7

Results

7.1 Sensitivity Study for Classical Novae End-point Nuclides

An example of an abundance plot of stable isotopes is given in Fig. 7.1 and 7.2, in terms of mass number and mass fraction. mass fraction is defined as:

$$X_i = \frac{N_i M_i}{\rho N_A} \tag{7.1}$$

Where N_i is the number of species i per unit volume, M_i is the molar mass, N_A is Avagadro's number, $6.02x10^{23}$ and ρ is the mass density.

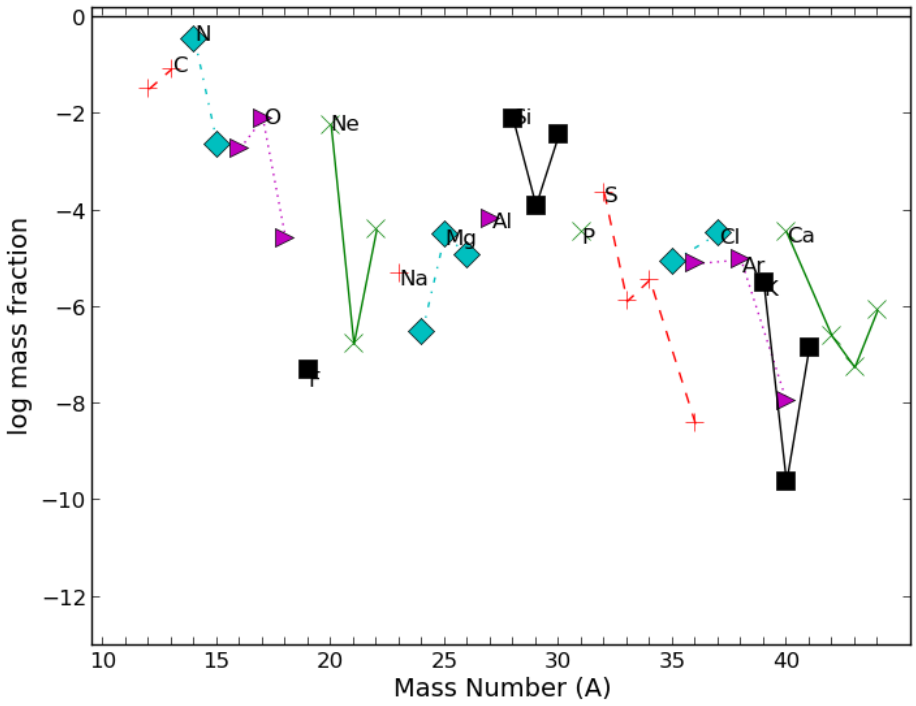

Figure 7.1 Abundance plot of stable isotopes of a CO nova with conditions described in Section 6.1. Mass fraction is plotted against the corresponding mass number, A, with specific isotopes denoted by colour

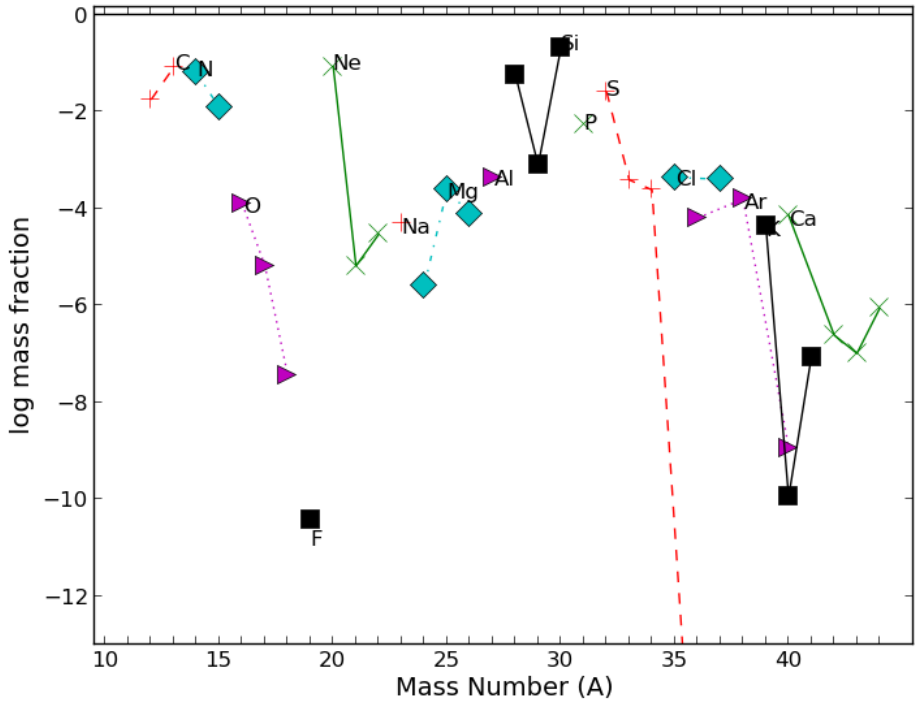

Figure 7.2 Abundance plot of stable isotopes of an ONe nova with conditions described in Section 6.1. Mass fraction is plotted against the corresponding mass number, A, with specific isotopes denoted by colour

The sensitivity study covered the (p,γ) reactions of $^{35-39}$Ar,$^{37-40}$K, $^{39-42}$Ca. The factor of change in relevant isotopes when varying reaction rates is tabulated and given in Tables 7.1 and 7.2. Only reactions that produced a factor of change of at least 1.5 times were considered for this table.

Table 7.1: Final Abundance Factor of Change Resulting from Reaction-Rate variations for CO Nova Model

		Reaction-Rate Multiplied by	
Reaction	Isotope	0.01	100
^{36}Ar(p,γ)			
	^{36}Ar	5.26	0.000883
	^{38}Ar	7.32	1.24
	^{39}K	0.99	1.02
^{37}Ar(p,γ)			
	^{38}Ar	0.73	4.22
	^{39}Ar	0.82	3.13
	^{39}K	0.99	1.20
^{38}Ar(p,γ)			
	^{38}Ar	1.13	0.25
	^{39}K	0.59	3.21
^{38}K(p,γ)			
	^{38}Ar	1.00	0.86
	^{39}K	0.99	1.43
^{39}K(p,γ)			
	^{39}K	1.02	0.16
	^{40}Ca	1.00	1.08
^{40}K(p,γ)			
	^{40}K	1.04	0.03

^{40}Ca(p,γ)			
	^{41}K	1.00	1.00
	^{42}Ca	1.00	1.00
^{42}Ca(p,γ)			
	^{42}Ca	1.01	0.28
	^{43}Ca	0.94	4.26

Table 7.2: Final Abundance Factor of Change Resulting from Reaction-Rate variations for ONe Nova Model

		Reaction-Rate Multiplied by	
Reaction	Isotope	0.01	100
^{36}Ar(p,γ)			
	^{36}Ar	9.21	0.01
	^{38}Ar	0.10	1.12
	^{39}K	0.33	1.09
^{37}Ar(p,γ)			
	^{38}Ar	0.02	3.16
	^{39}Ar	0.03	3.15
	^{39}K	0.28	2.29
^{38}Ar(p,γ)			
	^{38}Ar	1.12	0.70
	^{39}K	0.68	2.00
^{38}K(p,γ)			
	^{38}Ar	1.19	0.12
	^{39}K	0.40	3.73
^{39}K(p,γ)			
	^{39}K	1.26	0.06
	^{40}Ca	0.84	1.59
^{40}K(p,γ)			
	^{40}K	1.87	0.01

$^{40}\mathrm{Ca}(\mathrm{p},\gamma)$			
	$^{42}\mathrm{Ca}$	1.00	1.68
$^{42}\mathrm{Ca}(\mathrm{p},\gamma)$			
	$^{42}\mathrm{Ca}$	1.26	0.01
	$^{43}\mathrm{Ca}$	0.44	3.01

Chapter 8

Discussion

8.1 Sensitivity Study for Classical Novae End-point Nuclides

Of the reactions whose rates were varied, those that caused a factor of change in the final abundances of an isotope of at least 1.5 times were tabulated in Tables 7.2 and 7.1. The next step at the time of writing is to investigate existing studies on these reaction rates in order to identify which reaction rates require further examination.

The reactions of interest which had the greatest impact on the final abundances, were the (p,γ) reactions of ^{36}Ar,^{37}Ar and ^{40}K. These had abundance changes that were more than an order of magnitude for various isotopes, as shown in the semi-log plots in Fig. 8.1,8.2, and 8.3.

The next step is to search through literature in order to figure out what existing measurements there are, for these reaction rates. If there is a need to measure the reaction rates more thoroughly, an experiment can be proposed for a lab such as DRAGON (Detector of Recoils And Gammas Of Nuclear

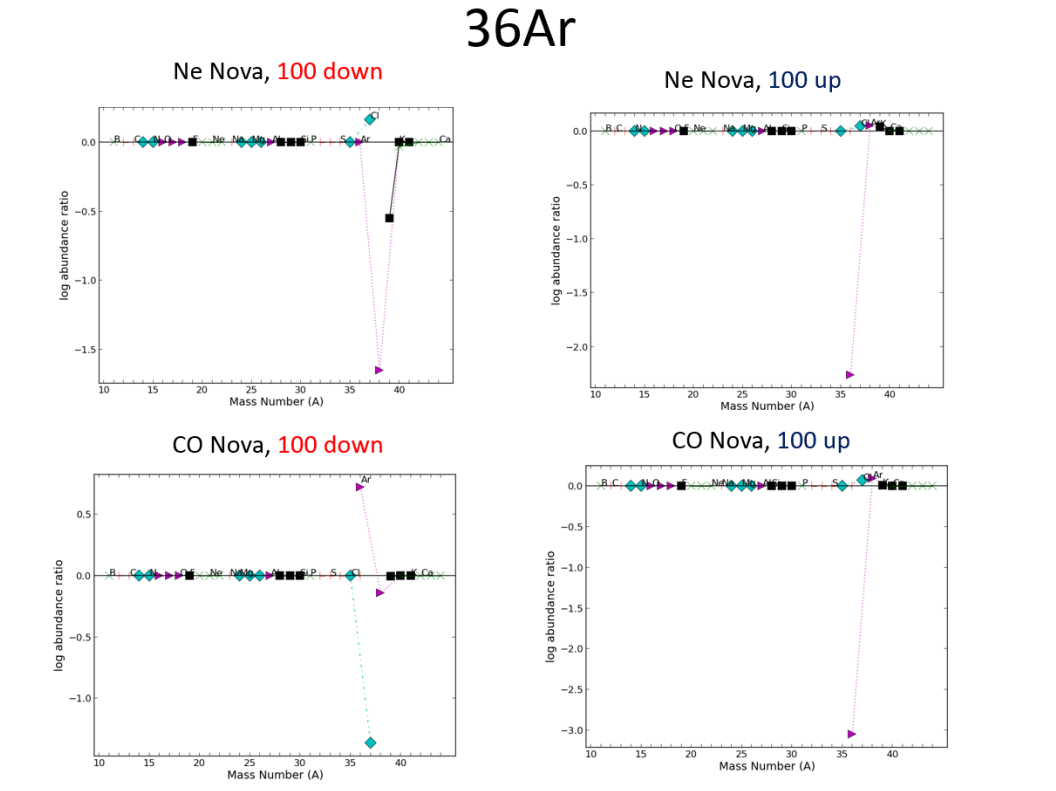

Figure 8.1 Abundance ratio between a simulation with the reaction rate of ^{36}Ar(p,γ) altered by a factor of 100 and the baseline simulation.

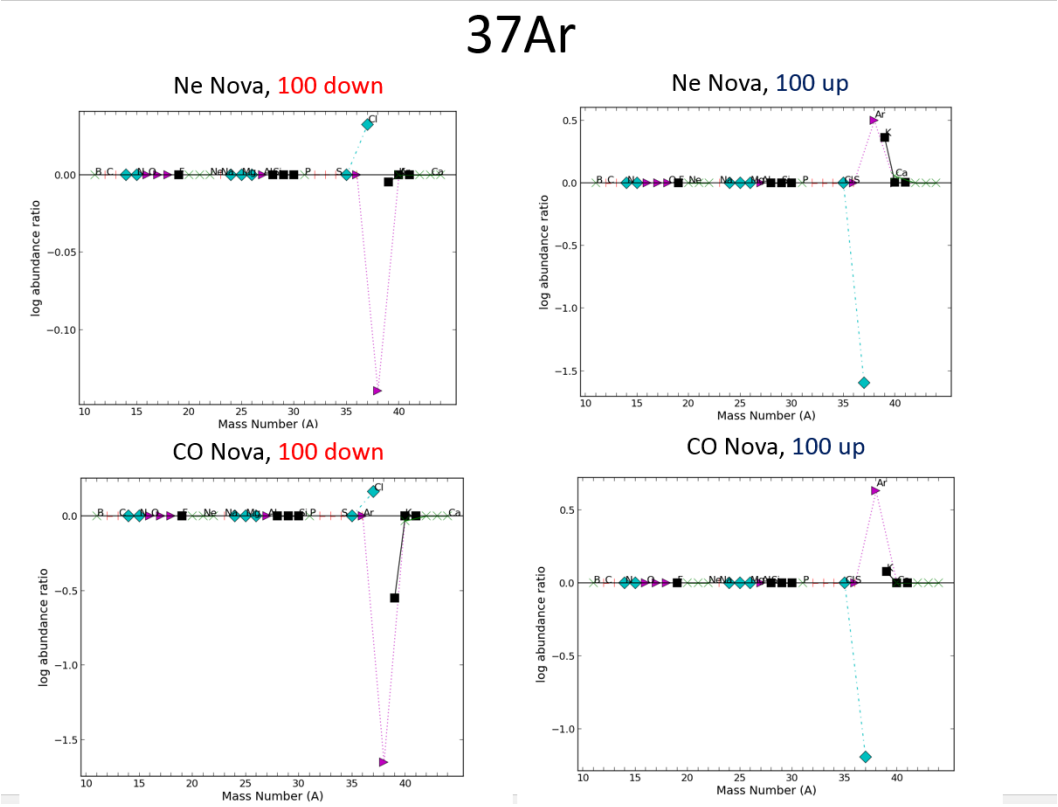

Figure 8.2 Abundance ratio between a simulation with the reaction rate of ^{37}Ar(p,γ) altered by a factor of 100 and the baseline simulation.

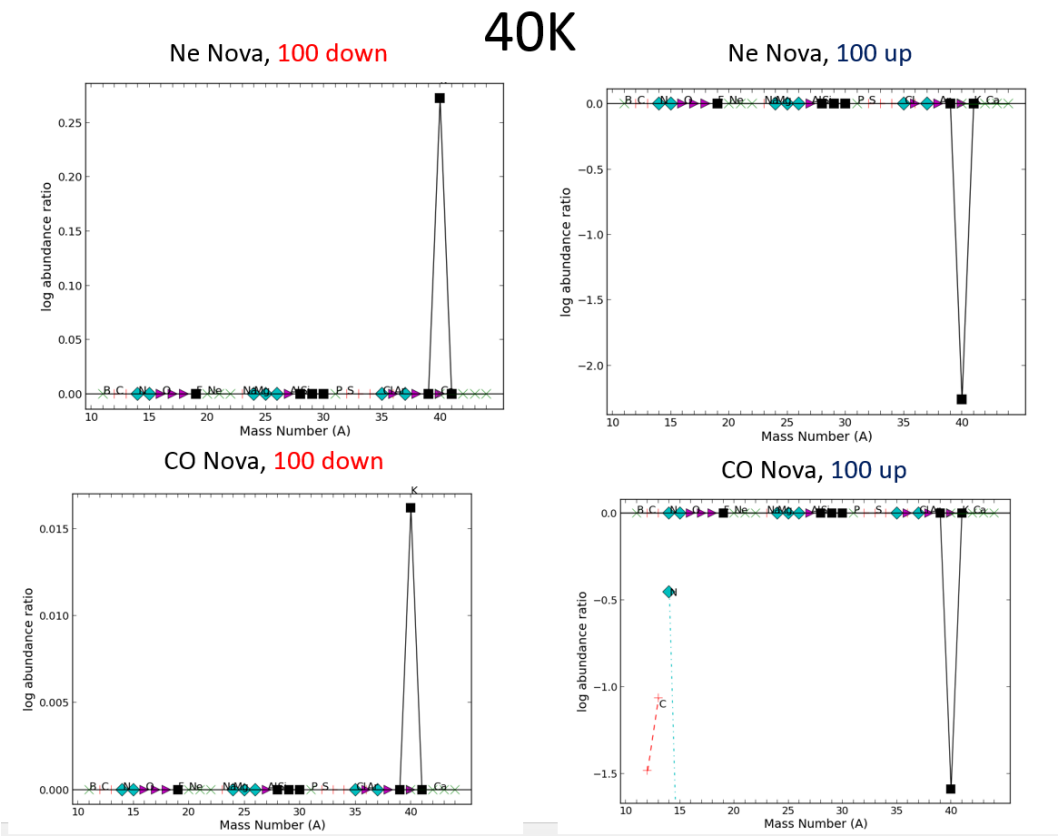

Figure 8.3 Abundance ratio between a simulation with the reaction rate of ^{40}K(p,γ) altered by a factor of 100 and the baseline simulation.

reactions) at TRIUMF, which can measure the resonance strength for (p,γ) reactions in inverse kinematics with stable or radioactive beams. Alternatively, an experiment can be done at the Triangle Universities Nuclear Laboratory (TUNL) to study the structure of states in the compound nucleus that are important for (p,γ) reactions, using a split pole spectrograph and transfer reactions.

Chapter 9

Conclusion

Two aspects of nucleosynthesis far from stability, in the context of astrophysics, were examined. For neutron rich nuclides, the production of these nuclides and isotopic abundances are largely controlled by the s-process and r-process. For the r-process; an important mechanism within the framework of this model is β^- - delayed neutron emission. This phenomenon acts as a branching mechanism that shifts the abundance flow to adjacent isotopic chains, and plays a role in determining the final abundances. Theoretical calculations of delayed neutron probabilities have been attempted but do not repoduce experimental values accurately. A semi-empirical formula can be adopted, using systematics from experimental values. To this end, a compilation and evaluation of experimental data regarding P_n and half lives for β-delayed neutron emitters in literature was performed. This work covered the region $30 \leq Z \leq 40,49,50$ examining approximately 150 nuclides and evaluating over 200 papers. Two different methods of identifying systematics were compared; an improved method of systematics proposed by McCutchan et al. was compared to the Kratz-Herrmann formula, wherein the McCutchan et al. method produced fits that were significantly more accurate. Future plans for

this project are to thorougly evaluate the data in the $29 \leq Z \leq 57$ region and produce a single set of recommended values for P_n and $T_{1/2}$ to be published in Nuclear Data Sheets. For proton rich nuclides, a sensitivity study concerning nucleosynthesis for endpoint nuclei in classical novae was carried out. Simulations of classical novae were performed using NuGrid and MESA, and reaction rates were adjusted by factors of 100 one at a time to see their effects on the final abundance. This narrowed down the number of relevant reactions, and will be further studied, with a goal of reducing the uncertanties of the most sensitive reaction rates.

This page intentionally left blank.

Bibliography

Amiel, S. & Feldstein, H. 1970, Physics Letters B, 31, 59

Arcones, A. & Martínez-Pinedo, G. 2011, Phys. Rev. C, 83, 045809

Birch, M., Singh, B., Dillmann, I., Abriola, D., Johnson, T., McCutchan, E., & Sonzogni, A. 2015, Nuclear Data Sheets, 128, 131

Borzov, I. 2003, Physical Review C, 67, 025802

Caballero-Folch, R., Domingo-Pardo, C., Agramunt, J., Algora, A., Ameil, F., Arcones, A., Ayyad, Y., Benlliure, J., Borzov, I. N., Bowry, M., Calviño, F., Cano-Ott, D., Cortés, G., Davinson, T., Dillmann, I., Estrade, A., Evdokimov, A., Faestermann, T., Farinon, F., Galaviz, D., García, A. R., Geissel, H., Gelletly, W., Gernhäuser, R., Gómez-Hornillos, M. B., Guerrero, C., Heil, M., Hinke, C., Knöbel, R., Kojouharov, I., Kurcewicz, J., Kurz, N., Litvinov, Y. A., Maier, L., Marganiec, J., Marketin, T., Marta, M., Martínez, T., Martínez-Pinedo, G., Montes, F., Mukha, I., Napoli, D. R., Nociforo, C., Paradela, C., Pietri, S., Podolyák, Z., Prochazka, A., Rice, S., Riego, A., Rubio, B., Schaffner, H., Scheidenberger, C., Smith, K., Sokol, E., Steiger, K., Sun, B., Taín, J. L., Takechi, M., Testov, D., Weick, H., Wilson, E., Winfield, J. S., Wood, R., Woods, P., & Yeremin, A. 2016, Phys. Rev. Lett., 117, 012501

Cowan, J., Cameron, A., & Truran, J. 1982, The Astrophysical Journal, 252, 348

Denissenkov, P. A., Herwig, F., Bildsten, L., & Paxton, B. 2013, The Astrophysical Journal, 762, 8

Denissenkov, P. A., Truran, J. W., Pignatari, M., Trappitsch, R., Ritter, C., Herwig, F., Battino, U., Setoodehnia, K., & Paxton, B. 2014, MNRAS, 442, 2058

Denissenkov, P. A., Truran, J. W., Pignatari, M., Trappitsch, R., Ritter, C., Herwig, F., Battino, U., Setoodehnia, K., & Paxton, B. 2014, Monthly Notices of the Royal Astronomical Society, 442, 2058

Duke, C., Hansen, P., Nielsen, O., & Rudstam, G. 1970, Nuclear Physics A, 151, 609

Duncan, R. C., Shapiro, S. L., & Wasserman, I. 1986, ApJ, 309, 141

Fulton, B. R. 2011, Journal of Physics: Conference Series, 312, 052001

GARVEY, G. T., GERACE, W. J., JAFFE, R. L., TALMI, I., & KELSON, I. 1969, Rev. Mod. Phys., 41, S1

Iliadis, C. 2015, Nuclear Physics of Stars, 2nd edn. (Wiley-VCH)

Iliadis, C., Champagne, A., JosÃľ, J., Starrfield, S., & Tupper, P. 2002, The Astrophysical Journal Supplement Series, 142, 105

JosÃľ, J. & Hernanz, M. 2007, Journal of Physics G: Nuclear and Particle Physics, 34, R431

Klapdor, H. 1983, Progress in Particle and Nuclear Physics, 10, 131

Kratz, K.-L., Bitouzet, J.-P., Thielemann, F.-K., Moeller, P., & Pfeiffer, B. 1993, ApJ, 403, 216

Kratz, K. L. & Herrmann, G. 1973, Zeitschrift für Physik, 263, 435

Lotay, G., Christian, G., Ruiz, C., Akers, C., Burke, D. S., Catford, W. N., Chen, A. A., Connolly, D., Davids, B., Fallis, J., Hager, U., Hutcheon, D. A., Mahl, A., Rojas, A., & Sun, X. 2016, Phys. Rev. Lett., 116, 132701

Madland, D. G. & Nix, J. 1988, Nuclear Physics A, 476, 1

Marketin, T., Huther, L., & Martínez-Pinedo, G. 2016a, Physical Review C, 93, 025805

Marketin, T., Huther, L., & Martínez-Pinedo, G. 2016b, Phys. Rev. C, 93, 025805

McCutchan, E. A., Sonzogni, A. A., Johnson, T. D., Abriola, D., Birch, M., & Singh, B. 2012, Phys. Rev. C, 86, 041305

Moller, P., Nix, J., Myers, W., & Swiatecki, W. 1995, Atomic Data and Nuclear Data Tables, 59, 185

Mumpower, M., Surman, R., McLaughlin, G., & Aprahamian, A. 2016, Progress in Particle and Nuclear Physics, 86, 86

Pappas, A. & Sverdrup, T. 1972, Nuclear Physics A, 188, 48

Parikh, A., José, J., & Sala, G. 2014, AIP Advances, 4, 041002

Pfeiffer, B., Kratz, K.-L., & MÃűller, P. 2002, Progress in Nuclear Energy, 41, 39

Pfeiffer, B., Kratz, K.-L., & Moller, P. 2001

Potekhin, A. Y. & Chabrier, G. 2010, Contributions to Plasma Physics, 50, 82

Rogers, F. J. & Nayfonov, A. 2002, ApJ, 576, 1064

Saha, M. N. 1920, The London, Edinburgh, and Dublin Philosophical Magazine and Journal of Science, 40, 472

Satchler, G. 1990, Introduction to Nuclear Reactions, 2nd edn. (Palgrave)

Saumon, D., Chabrier, G., & van Horn, H. M. 1995, ApJS, 99, 713

Setoodehnia, K. 2011, PhD thesis, Thesis–McMaster University

Sneden, C. & Cowan, J. J. 2003, Science, 299, 70

Sneden, C., Cowan, J. J., & Gallino, R. 2008, Annu. Rev. Astron. Astrophys., 46, 241

Starrfield, S., Timmes, F., Iliadis, C., Hix, W., Arnett, W. D., Meakin, C., & Sparks, W. 2012, arXiv preprint arXiv:1211.6145

Thompson, I. J. & Nunes, F. M. 2009, Nuclear Reactions for Astrophysics: Principles, Calculation and Applications of Low-Energy Reactions, 1st edn. (Cambridge University Press)

Timmes, F. X. & Swesty, F. D. 2000, The Astrophysical Journal Supplement Series, 126, 501

Zhi, Q., Caurier, E., Cuenca-García, J. J., Langanke, K., Martínez-Pinedo, G., & Sieja, K. 2013, Phys. Rev. C, 87, 025803

This page intentionally left blank.